Electronic Supplementary Information (ESI) for

A high performance oxygen storage material for chemical looping processes with CO_2 capture

Qilei Song,*[ab] Wen Liu,[a] Christopher D. Bohn,[a] Ryan N. Harper,[c] Easan Sivaniah,[b] Stuart A. Scott,[c] and John S. Dennis*[a]

[a] Department of Chemical Engineering and Biotechnology, University of Cambridge, Cambridge CB2 3RA, UK. Fax: 0044 1223334796; Tel: 0044 1223 334787; Email: jsd3@cam.ac.uk (J.S. Dennis)

[b] Cavendish Laboratory, University of Cambridge, Cambridge CB3 0HE, UK. Fax: 0044 1223 337000; Tel: 0044 1223 337010; Email: qs209@cam.ac.uk (Q.L. Song)

[c] Department of Engineering, University of Cambridge, Cambridge CB2 1PZ, UK

***Author to whom correspondence should be addressed.**

Table of Contents

1. Methods

1.1 Materials

Copper nitrate pentahydrate [$Cu(NO_3)_2 \cdot 2.5H_2O$, purity 98 wt%], aluminium nitrate nonahydrate [$Al(NO_3)_3 \cdot 9H_2O$, purity 98 wt%], NaOH (anhydrous purity 99 wt%), and Na_2CO_3 (anhydrous purity 99 wt%) were purchased from Fisher Scientific and used as received. Purified water from reverse osmosis was used for the synthesis of LDHs. Zero grade N_2, dilute CO in N_2 (20 vol%), dilute H_2 in N_2 (5 vol%) and zero grade air were supplied by BOC.

1.2 Synthesis of Cu-Al layered double hydroxides precursor

Cu-Al LDH precursor was synthesised by co-precipitation, at room temperature and atmospheric pressure and a constant, controlled pH. A representative protocol is described below. Aqueous solutions of 1M $Cu(NO_3)_2 \cdot 2.5H_2O$ and 1 M $Al(NO_3)_3 \cdot 9H_2O$ and the precipitating agent, a mixture of NaOH and Na_2CO_3 (1 M of each), were co-added dropwise to an empty flask with vigorous stirring. The pH of the slurry was maintained at 9.6 ± 0.1 by adjusting the pumping rates of both solutions. The greenish-blue precipitate was then aged without stirring for 2 h at room temperature, followed by filtration, washing with deionised water five times at room temperature to ensure that the conductivity of the slurry had fallen below 120 $\mu S \cdot cm^{-1}$. The precipitate was then filtered and dried in an oven at 60°C in air for 48 h. The dried precursor was then calcined in a muffle furnace in air at 950°C, after being from room temperature to 950°C at a heating rate of about 10°C/min. The total calcination time (including heating up) was 5 h. After cooling to room temperature, the calcined materials were crushed and sieved to a particle size of 500-710 μm.

Samples with different concentrations of CuO (from 20-100 wt%) in mixture with Al_2O_3 were prepared by changing the molar ratio of $Cu^{2+}:Al^{3+}$ in the solution with total concentration of Cu and Al equal to 1 M. Additionally, two series of LDH precursors, with fixed $Cu^{2+}:Al^{3+}$ atomic ratios of either 1:1 or 3:1 were prepared, whilst varying the ratios of [NaOH]:[Na_2CO_3] for each as follows: 1:0, 0.94:0.06, 0.5:0.5, and 0:1. The total concentration, *i.e.* [NaOH] + [Na_2CO_3], was fixed at 1 M throughout.

1.3 Fluidised bed apparatus

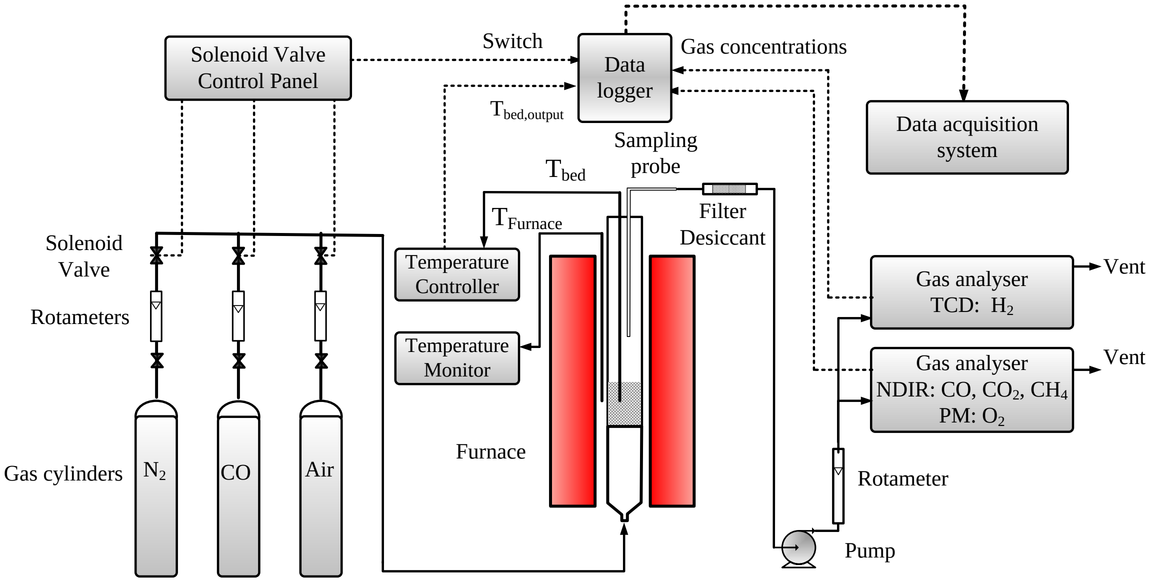

Fig. S1 Schematic diagram of the fluidised bed apparatus. NDIR: non-dispersive infrared analyser; PM: paramagnetic analyser; TCD: Thermal conductivity.

The kinetics and performance of looping reactions were investigated in a laboratory fluidised bed as shown in Fig. S1. The reactor (i.d. 29.5 mm; length 460 mm) was made of quartz with a sintered porous quartz plate as gas distributor located 110 mm from the bottom. The reactor was heated by an electric furnace and the temperature of the bed was controlled by a PID controller connected to a K-type thermocouple situated axially in the bed 15 mm above the distributor. A second K-type thermocouple was placed at the same position to log temperature continuously. Gases were supplied to the reactor from gas cylinders metered to the bed by rotameters via solenoid valves, allowing gases to be switched.

The flue gas was sampled from a point 140 mm above the gas distributor *via* a quartz sampling probe and desiccating tubes containing $CaCl_2$ with quartz wool as a filter at both ends. The resulting dry gas was introduced to two continuous gas analysers placed in parallel with a flow rate of 0.5 L/min (at 293 K and 1 atm) passing to each. The first analyser (ABB EL3020) measured [CO_2], [CH_4], [CO] (via non-dispersive infrared (NDIR)) and [O_2] (using a paramagnetic method); the detection limit was 0.01 vol%. The second analyser (ABB EL3020) (not used in this study) measured the mole fraction of H_2 using the principle of thermal conductivity (TCD). The concentrations were recorded at a frequency of 0.5 Hz in most experiments. The time delay of each analyser to a step change of gas in the inlet valves was around 13.0-16 s, after which the time taken to reach steady state was approximately first-order with time constants of 2.7 s for CO, CO_2, and CH_4, 3.0 s for O_2 and 1.0 s for H_2, respectively. These time constants were used to correct the raw measurements for the first-order mixing in the sampling system. In continuous measurements, the time delay was subtracted from the results of concentration against time, so as to correlate changes in concentration with changes in measured temperature.

1.4 Cyclic oxygen release and storage in a fluidised bed

Cycles of O_2 release and uptake by the solids were undertaken by exposing the materials to alternating decomposing and oxidising atmospheres in the laboratory-scale fluidised bed. In a typical first cycle, a batch of 15 g of oxygen carrier (without other bed materials) was heated in the fluidised bed to the desired reaction temperature, fluidised by zero grade air (47.4 mL/s, at measured at STP). Next, the fluidising gas was switched to pure N_2 (50.0 mL /s, at STP) and the concentration of oxygen in the off-gas was measured continuously for 360 s. After this, the fluidising gas was switched to air (47.4 mL/s, STP), and, again, the concentration of oxygen in the exit gas was monitored for between 360 and 720 s, depending on the operating temperature, which was varied between 700 and 1000°C. The cycle was then repeated. By analysing the profile of the off-gas concentration with respect to time, it was possible to determine the apparent rate and extent of oxygen release, and the stability of these parameters over multiple cycles. In the case of the decomposition-oxidation cycles, the molar fractional decomposition of the CuO to Cu_2O, $X_{\mathrm{OC,red}}$ in the carrier up to time t_i was calculated as:

$$X_{\mathrm{OC,red}} = \frac{4M_{\mathrm{CuO}}}{m_{\mathrm{ox}} x_{\mathrm{CuO}}} \int_0^{t_\mathrm{i}} (\dot{n}_{\mathrm{out}} y_{\mathrm{O_2,out}}) dt \qquad \text{(S1)}$$

where M_{CuO} is the molecular weight of CuO, g/mol, x_{CuO} is the mass fraction of CuO in the oxygen carrier, and m_{ox} is the initial mass of the oxygen carrier in the bed in g, $y_{\mathrm{O_2,out}}$ is the mole fraction of O_2 in the effluent gas, and $\dot{n}_{\mathrm{out}}$ is the total molar flow rate of the effluent gas in mol/s.

1.5 Cyclic reduction and oxidation in a fluidised bed

In order to evaluate the stability of the oxygen carrier materials when used in the presence of a gaseous fuel (CO), multiple cycles of reduction and oxidation were performed in the fluidised bed. In this experiment, the bed material consisted of 20 mL of alumina sand (300-425 µm) to which 0.5 g of oxygen carrier material (500-710 µm) was added. Then the bed was heated to the desired reaction temperature (typically ~ 950°C), fluidised by air. The oxygen carrier particles were exposed to about 20 consecutive redox cycles with each cycle consisting of four stages: (1) purging with inert N_2 (50.0 mL/s, STP), (2) reduction of the oxygen-carrier in ~2.4 vol% CO in N_2 for 180 s (total flow rate of 65.8 mL/s, STP), (3) purging with inert N_2 for 90 s (50.0 mL/s, STP), (4) oxidation with air for 180 s (47.4 mL/s, STP). For these experiments, the oxygen carrier conversion, defined as the ratio of the measured number of moles of CO_2 produced to the number expected from the complete reduction of the given mass of CuO to Cu in the carrier by CO, was used to check the mass balance of oxygen:

$$X_{\mathrm{red}} = \frac{M_{\mathrm{CuO}}}{m_{\mathrm{ox}} y_{\mathrm{CuO}}} \int_0^{t} \dot{n}_{\mathrm{out}} y_{\mathrm{CO_2}} dt \qquad \text{(S2)}$$

where $y_{\mathrm{CO_2}}$ is the mole fraction of CO_2 in the product gas.

2. Characterisation of the Cu-Al-LDH precursor and derived mixed metal oxides

2.1 FTIR spectra (Fig. S2)

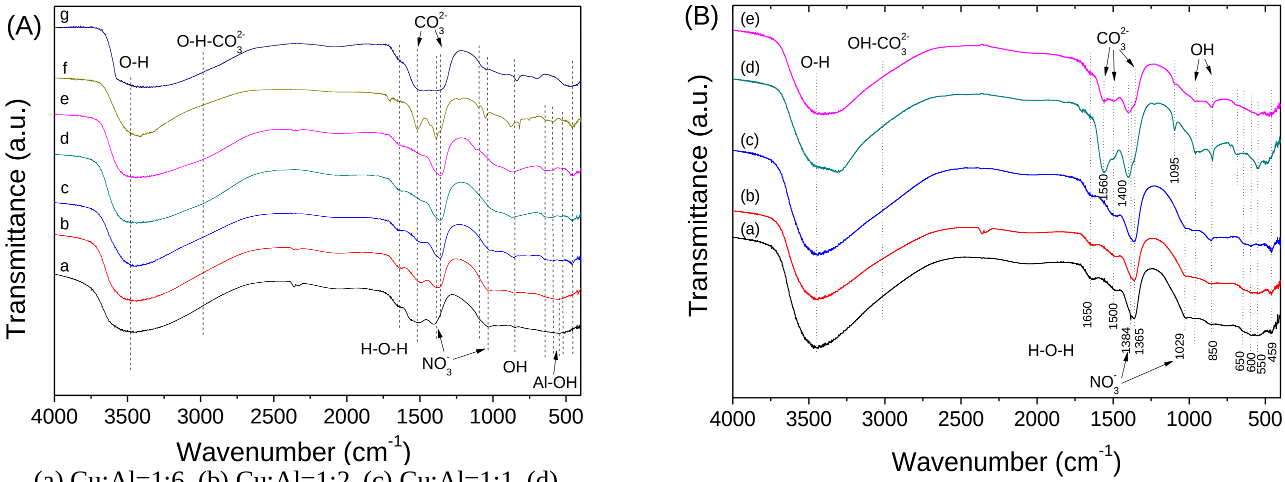

(a) Cu:Al=1:6, (b) Cu:Al=1:2, (c) Cu:Al=1:1, (d) Cu:Al=1.5:1, (e) Cu:Al=2:1, (f) Cu:Al=3:1, (g) Cu:Al=1:0. [Cu]+[Al]=1 M; Precipitating agent: 0.5 M NaOH and 0.5 M Na_2CO_3.

(a)1 M NaOH, (b) 0.94 M NaOH+0.06 M Na_2CO_3, (c) 0.5 M NaOH+ 0.5 M Na_2CO_3, (d) 1 M NaOH+ 1 M Na_2CO_3, (e) 1 M Na_2CO_3. Molecular ratio of Cu:Al=1:1, [Cu]+[Al]=1 M.

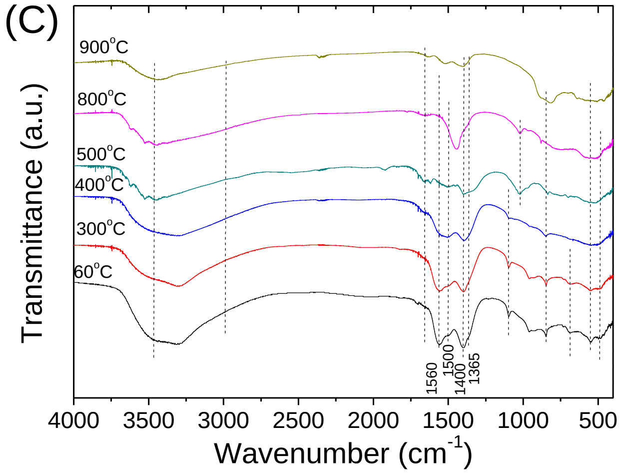

Fig. S2 FTIR spectra of precursors and calcined product. (A) precursor with varied Cu:Al molar ratio. (B) LDH precursors with Cu:Al=1:1 prepared with different alkaline solutions (NaOH+Na_2CO_3). (C) LDH precursor prepared from Cu:Al=1 M:1 M in mixture of NaOH and Na_2CO_3 (1 M of each) and sample after calcination at representative temperatures.

The broad absorption band in the 4000-3000 cm^{-1} region with peak at 3500 cm^{-1} is assigned to the OH stretching mode of the hydroxyl group, and interlayer water molecules. The shoulder at around 3000 cm^{-1} is OH stretching in H-bonded OH-CO_3^{2-}. The band at 1515 and 1650 cm^{-1} is due to H-O-H bending vibration for water adsorbed in the interlayers. The absorption peak at 1365 cm^{-1} is the CO_3^{2-} stretching mode. The shoulder at 1500 cm^{-1} is assigned to weak splitting of the carbonate υ_3 band. The shoulder near 1050 cm^{-1} is symmetry υ_1 mode of carbonate, due to lower symmetry by interaction of interlayer carbonate with other atoms. The evident narrow peaks at 1384 and 1029 cm^{-1} are due to NO_3^- anions adsorbed in the interlayers. The peaks at 980, 960, 850, 835, 775 and 615 cm^{-1} correspond to OH in the Cu-Al-(OH)x. The peaks at 400 – 800 cm^{-1} correspond to the lattice vibration modes of Al-O and O-Al-O, including well-known Al-OH mode at around 550 cm^{-1}, observed at lower Cu:Al ratio.

For the precursors prepared using different precipitants, the major difference between these samples are the peaks due to the anions of NO_3^- and CO_3^{2-}. Weak peaks belong to CO_3^{2-} can be observed for the sample prepared with NaOH as precipitant, which is possibly due to the absorption of CO_2 during drying process. At high concentration of Na_2CO_3 solution, we can observe an increase in the absorption at 1500 cm^{-1}, and appearance of a peak at 1560 cm^{-1} assigned to symmetric O=C=O stretching.

Calcination of the Cu-Al LDH precursor resulted in the weakening of peaks assigned to H-O-H, Cu-Al-OH, NO_3^- and CO_3^{2-}, corresponding to the structural evolution during thermal treatment.

2.2 XRD patterns of precursor and calcined product with various Cu-Al ratios (Fig. S3)

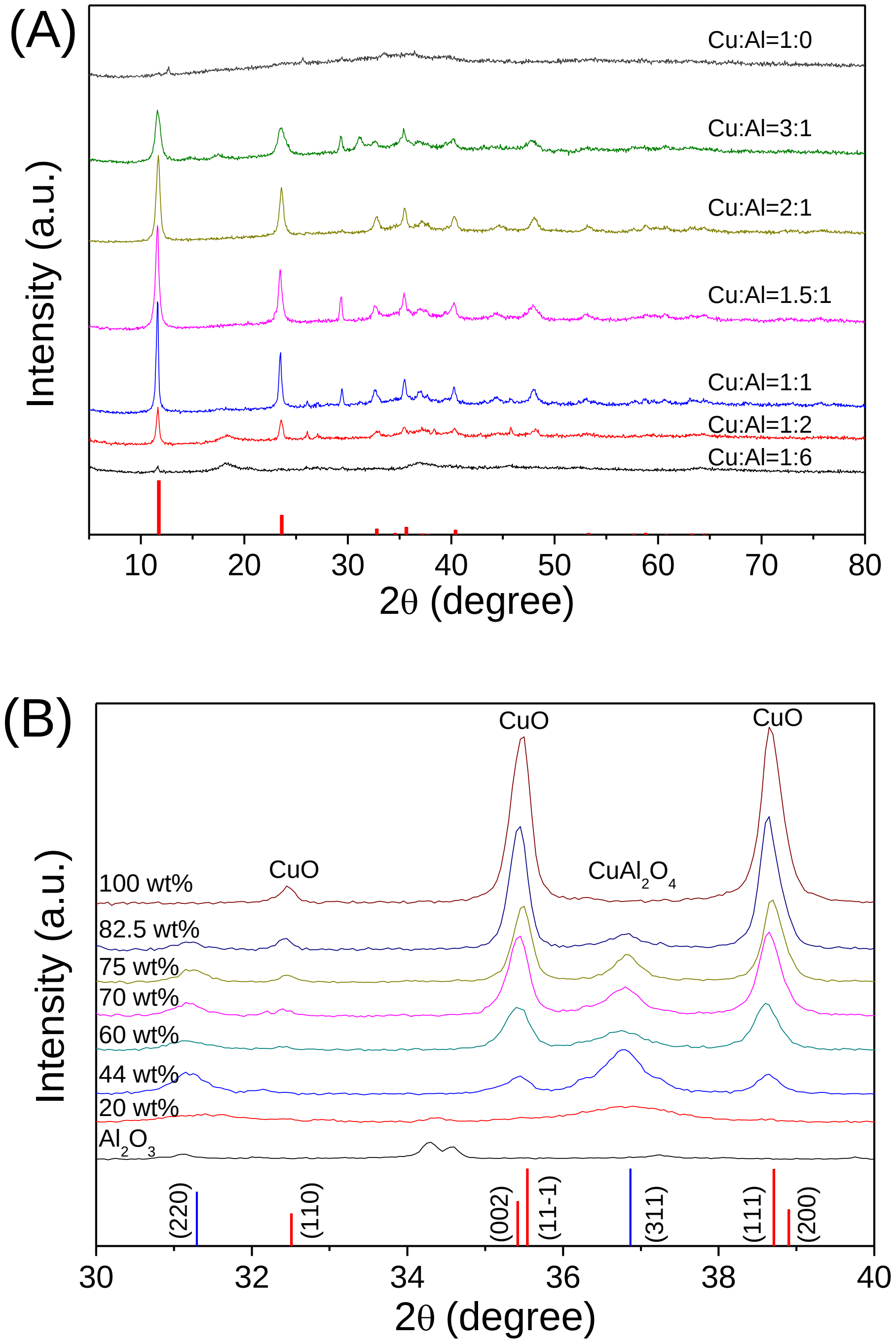

Fig. S3 XRD patterns of (A) as-synthesised precursor and (B) calcined product with different Cu^{2+}:Al^{3+} molecular ratios. [Cu]+[Al]=1 M. (A) The crystalline phase marked with vertical lines is hydrotalcite (JCPDS 46-0099). (B) The vertical lines correspond to patterns of CuO (Tenorite, JCPDS 48-1548, in red) and $CuAl_2O_4$ (JCPDS 33-0448, in blue), respectively. The precursors were prepared using a precipitating agent consisting of a mixture of NaOH and Na_2CO_3 (0.5 M of each).

$CuAl_2O_4$ was the dominant crystalline phase at low loadings of copper oxide, with CuO being the dominant phase at high loadings.

2.3 Thermal analyses of precursors prepared with various Cu-Al ratios (Fig. S4)

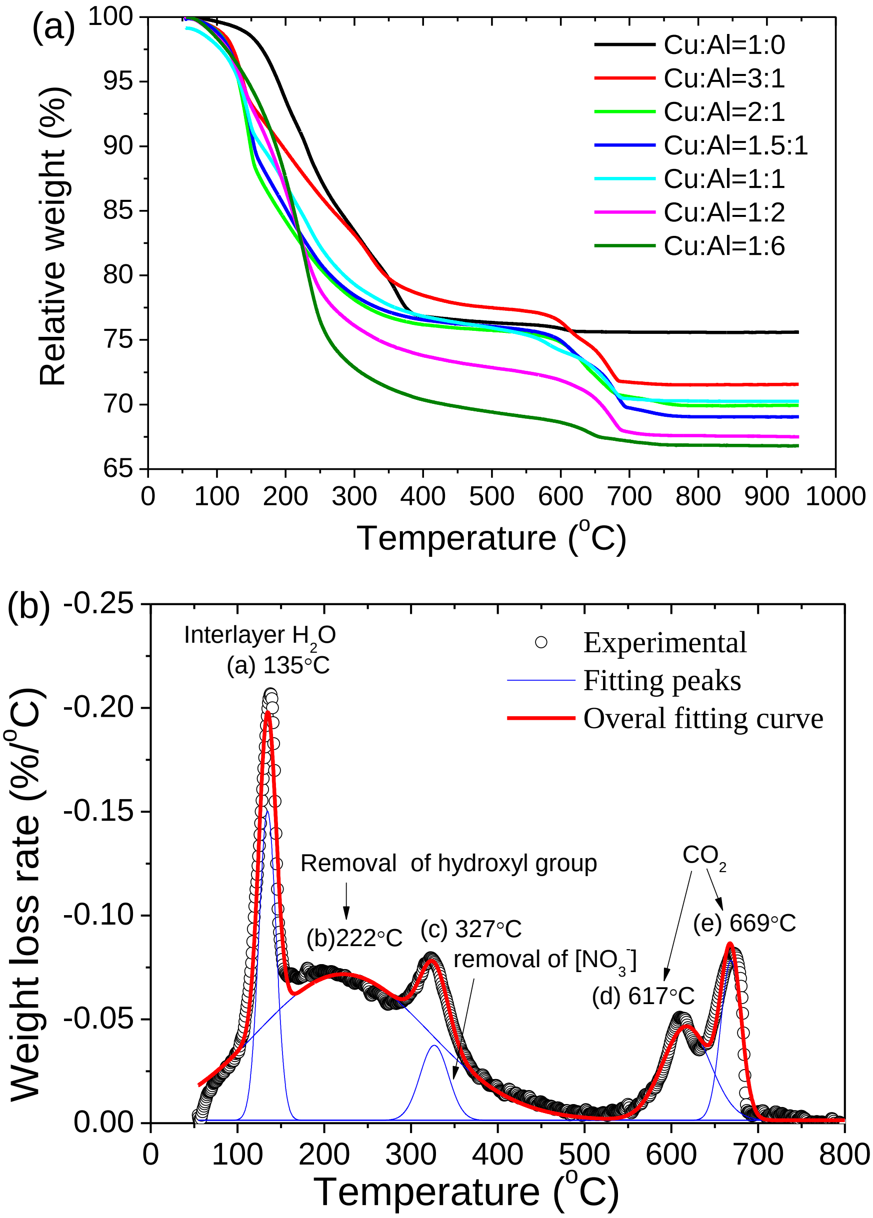

Fig. S4 Thermal analyses of LDH precursors prepared with various Cu:Al ratios at constant pH (9.5-9.7). The samples were heated at a rate of 10°C/min in air. (a) mass (b) derivative for the precursor with Cu:Al=3:1 showing the deconvolution. All samples were prepared using the same alkaline solution (0.5 M NaOH+0.5 M Na_2CO_3) by varying the molar ratio of Cu^{2+} to Al^{3+}. Total $[Cu^{2+}]+[Al^{3+}]=1$ M.

The decomposition follows the loss of (1) interlayer water at around 100-200°C, (2) removal of hydroxyl groups from the brucite layers, de-nitration and decarbonation over 100-400°C, (3) decomposition of the residual carbonate between 400-700°C.

The peaks of the time derivative of weight loss were simulated by fitting Gaussian curves (Fig. S4) to deconvolute the different stages of reaction. This gives an estimate of the relative amount of interlayer water and anions and thus providing an estimate of the molecular formula. For example, the precursor with a Cu^{2+}:Al^{3+} ratio of 3:1 was found to have a molecular formula of $Cu_{0.75}Al_{0.25}(OH)_2(NO_3)_{0.032}(CO_3)_{0.123}\cdot 0.143H_2O$, which is in close agreement with the theoretical form for an LDH.

2.4 Thermal analyses of the LDH precursor with varied precipitant (Fig. S5)

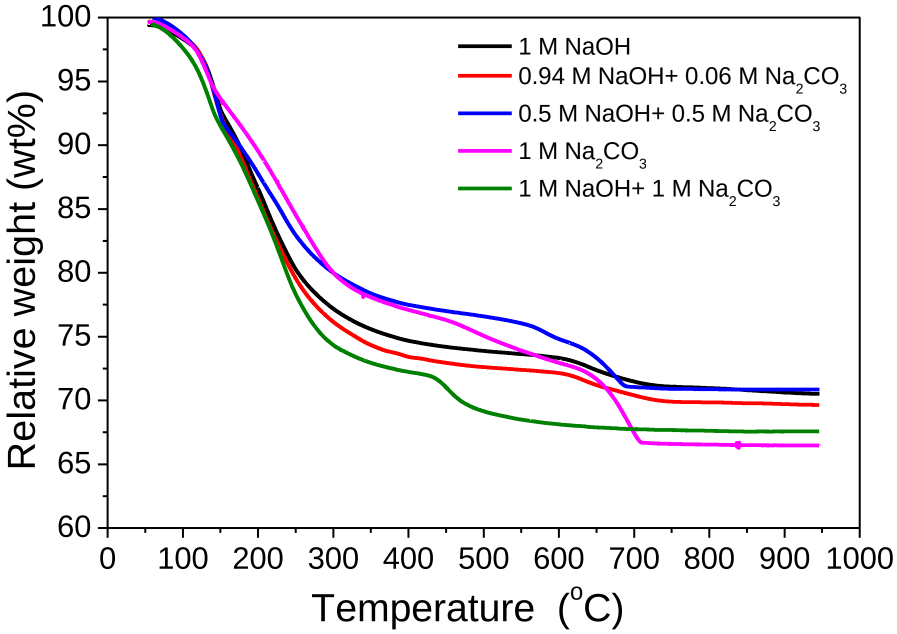

Fig. S5 Thermal analyses of LDH precursors prepared using various precipitants with Cu:Al=1:1.

2.5 XRD patterns of evolution of LDH precursor to mixed metal oxides upon calcination (Figs. S6-7)

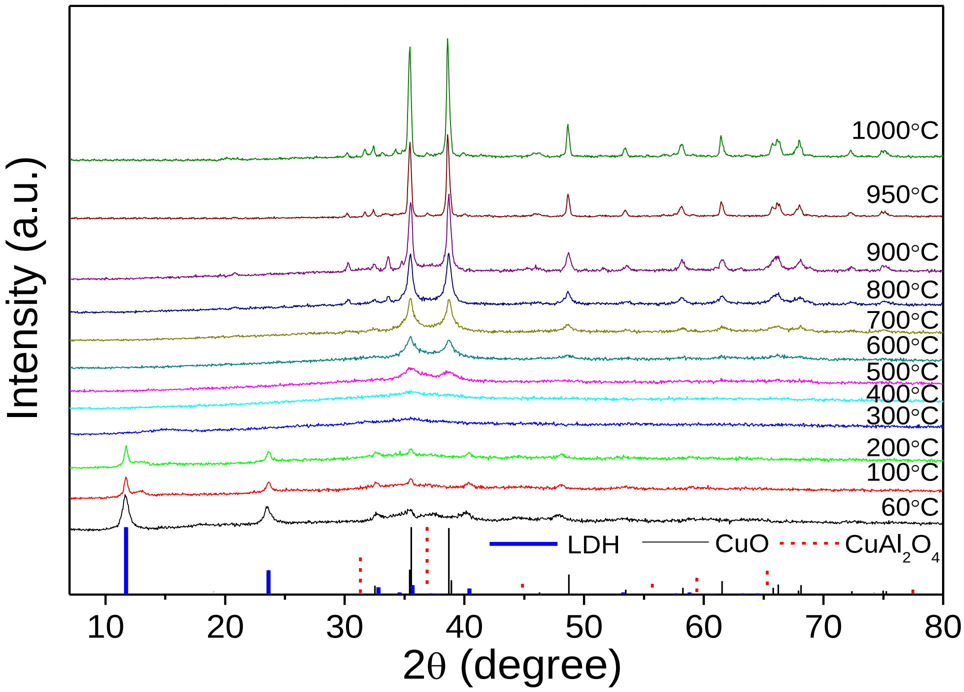

Fig. S6 *Ex situ* XRD patterns of the Cu-Al LDH precursor prepared with Cu^{2+}:Al^{3+}=1:1 with total concentration of 2 M, using a precipitant of mixture of NaOH and Na_2CO_3 (1 M of each) upon heating from 60°C to 1000°C in air. The crystalline patterns correspond to hydrotalcite (JCPDS 46-0099, blue vertical lines), CuO (Tenorite, JCPDS 48-1548, black vertical solid lines) and $CuAl_2O_4$ (JCPDS 33-0448, red vertical dashed lines), respectively.

Crystalline CuO was still the dominant phase even though the calcination temperature was increased up to 1000°C, with very weak peaks associated to $CuAl_2O_4$ or $CuAlO_2$.

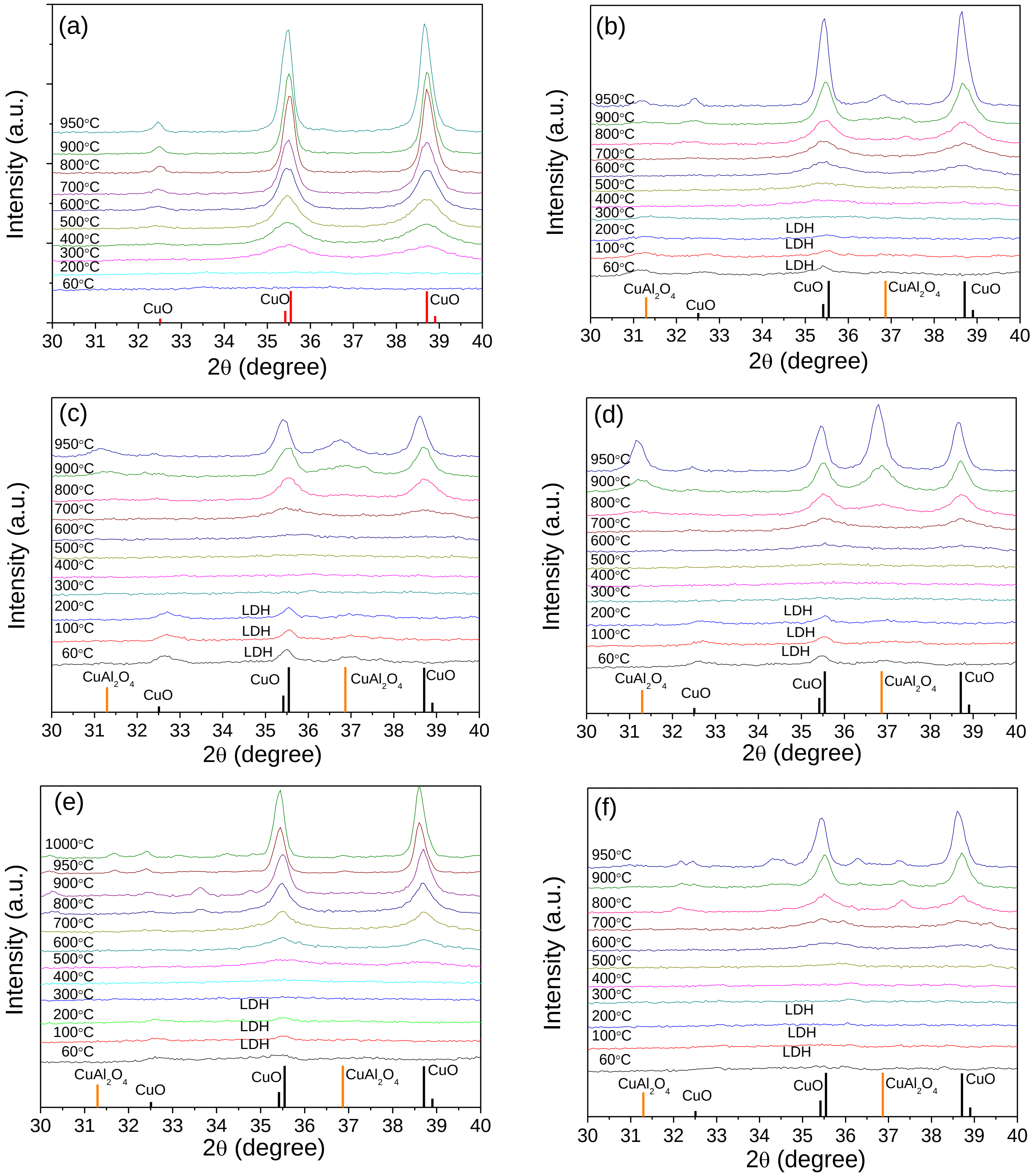

Fig. S7 Evolution of XRD patterns from precursor to metal oxides upon increasing calcination temperature. (a) Cu:Al=1:0, (b) Cu:Al=3:1, (c) Cu:Al=1:1, (a-c) using precipitant of NaOH and Na_2CO_3 (0.5 M of each). (d) Cu:Al=1:1, 1 M NaOH, (e) Cu:Al=1:1, 1 M NaOH+1 M Na_2CO_3, (f) Cu:Al=1:1, 1M Na_2CO_3. To clearly show crystalisation of CuO and $CuAl_2O_4$, only data within 2θ=30-40° are presented.

The precursor of pure CuO transformed to crystalline CuO at low temperature of 300°C, while the crystallisation of CuO in the Cu-Al LDH precursor did not occur until 600-700°C. Evident peaks of $CuAl_2O_4$ were observed at high annealing temperatures (above 800°C) when NaOH is the precipitating agent. In the case of samples prepared with higher concentrations of Na_2CO_3, the CuO was well dispersed in Al_2O_3, with the Al_2O_3 being amorphous and not detectable by X-ray diffraction.

2.6 SEM of Cu-Al LDH precursors prepared with various precipitants (Fig. S8)

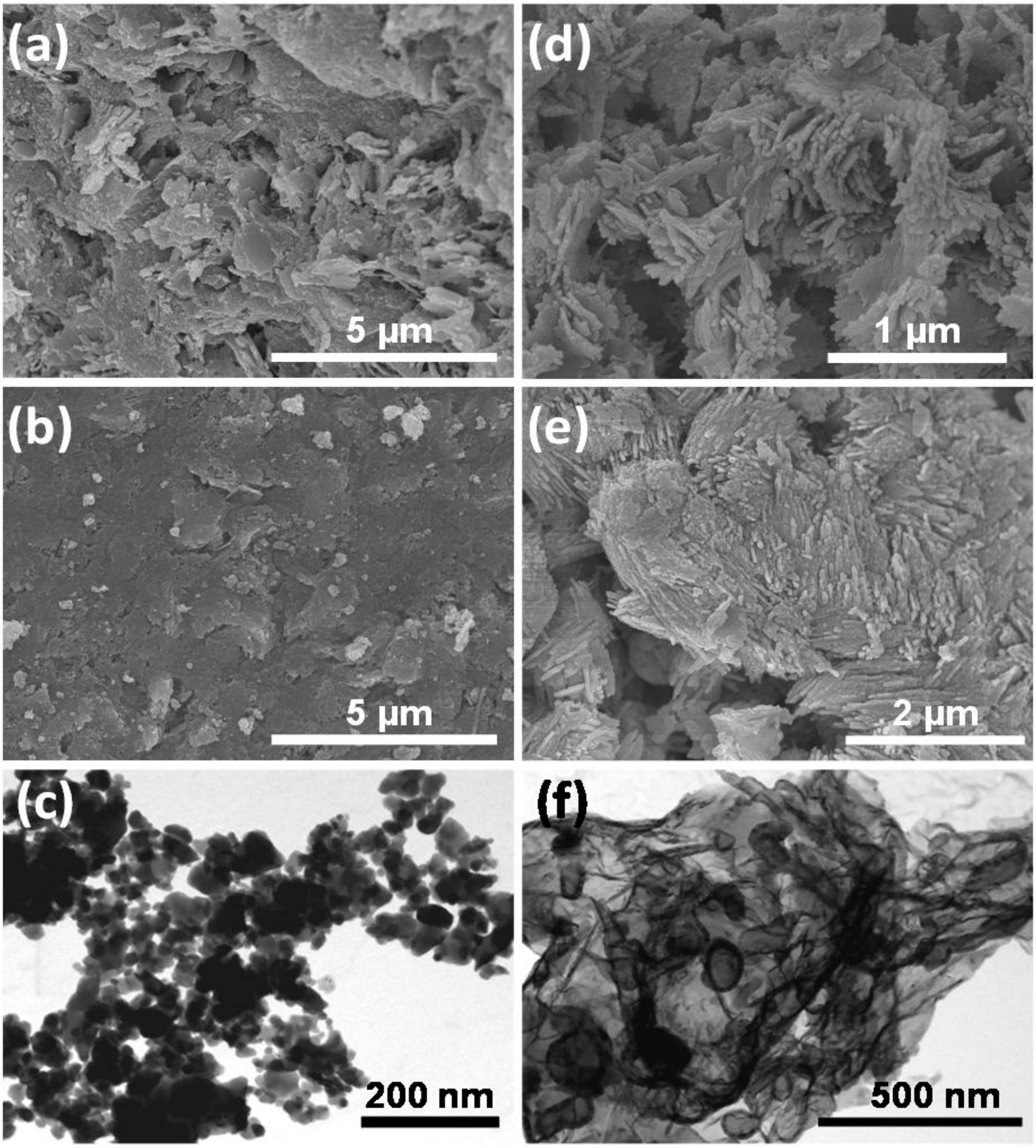

Fig. S8 Electron microscope images of (a,d) SEM of Cu-Al LDH precursor, (b,e) SEM and (c,f) TEM of calcined products prepared with Cu:Al=1:1 and different precipitants: (a-c) 1 M NaOH and (d-f) 1 M Na_2CO_3.

2.7 Correlation of composition of mixed metal oxides with precipitant (Fig. S9)

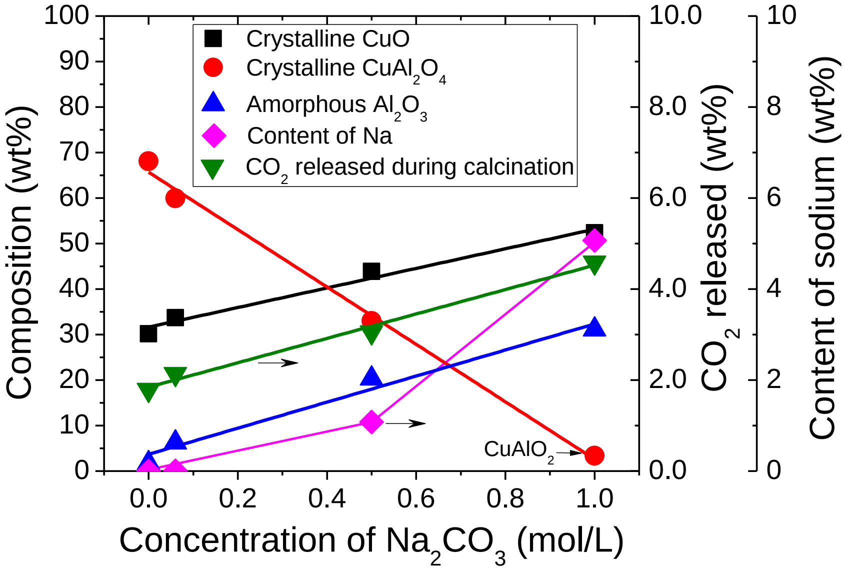

Fig. S9 Correlation of the composition of calcined product, residual content of sodium (wt % atomic sodium) with the concentration of Na_2CO_3 in the alkaline precipitating agent. The Cu:Al molar ratio was 1:1 with total concentration of 1 M, corresponding to nominal loading of 60 wt% CuO in the final product. The lines are added to guide the eyes.

2.8 Material chemistry of Cu-Al-LDH precursor prepared using increasing pH method (Fig. S10)

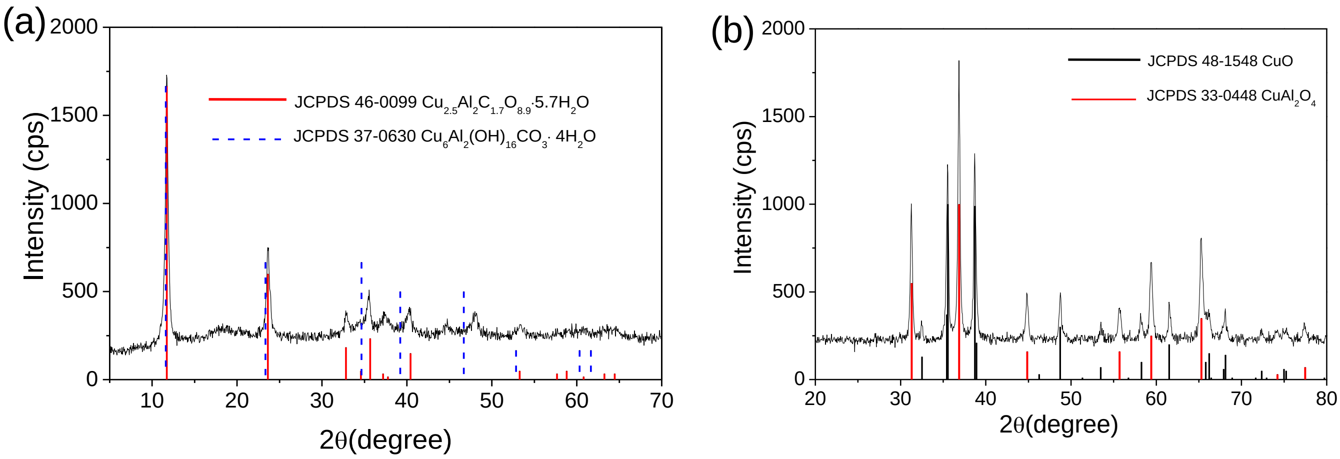

Fig. S10 XRD patterns of (a) Cu-Al LDH precursor and (b) calcined product prepared by sequential precipitation using increasing pH method.

Increasing pH method: The mixture of $Cu(NO_3)_2 \cdot 2.5H_2O$ (1 M) and $Al(NO_3)_3 \cdot 9H_2O$ solution (1 M) was prepared and a solution of NaOH (1 M) was added dropwisely until the pH reach to 3.9, and then another solution of Na_2CO_3 (1 M) was added dropwisely until the pH increased to around 9.7. The precipitate was aged for 2h at room temperature and then washed and filtered. The precipitate was then dried in oven for overnight. The calcination was carried out in a muffle oven in air at 950°C for 5 h. The content of sodium in both LDH precursor and calcined product were not detectable. XRD pattern confirmed the formation of Cu-Al LDH and the calcined product is a mixture of CuO and $CuAl_2O_4$. LDH is precipitated at lower pH consuming most of the Al, therefore, the formation of $NaAlCO_3(OH)_2$ was suppressed and the formation of $CuAl_2O_4$ was not hindered by $NaAlO_2$.

Decreasing pH method: Cu-Al nitrate solution was added dropwise to alkaline solution of NaOH and Na_2CO_3 with the pH decreasing from 13 to 9.7. In this case, malachite was observed by XRD, suggesting separate precipitation of Cu and Al, and the calcined product showed formation of $CuAl_2O_4$. In both cases, Na-containing species were not detected in XRD and ICP-AES confirmed that the absence of sodium in precursors and calcined products.

2.9 XRD patterns of aluminium precipitate and as calcined product (Fig. S11)

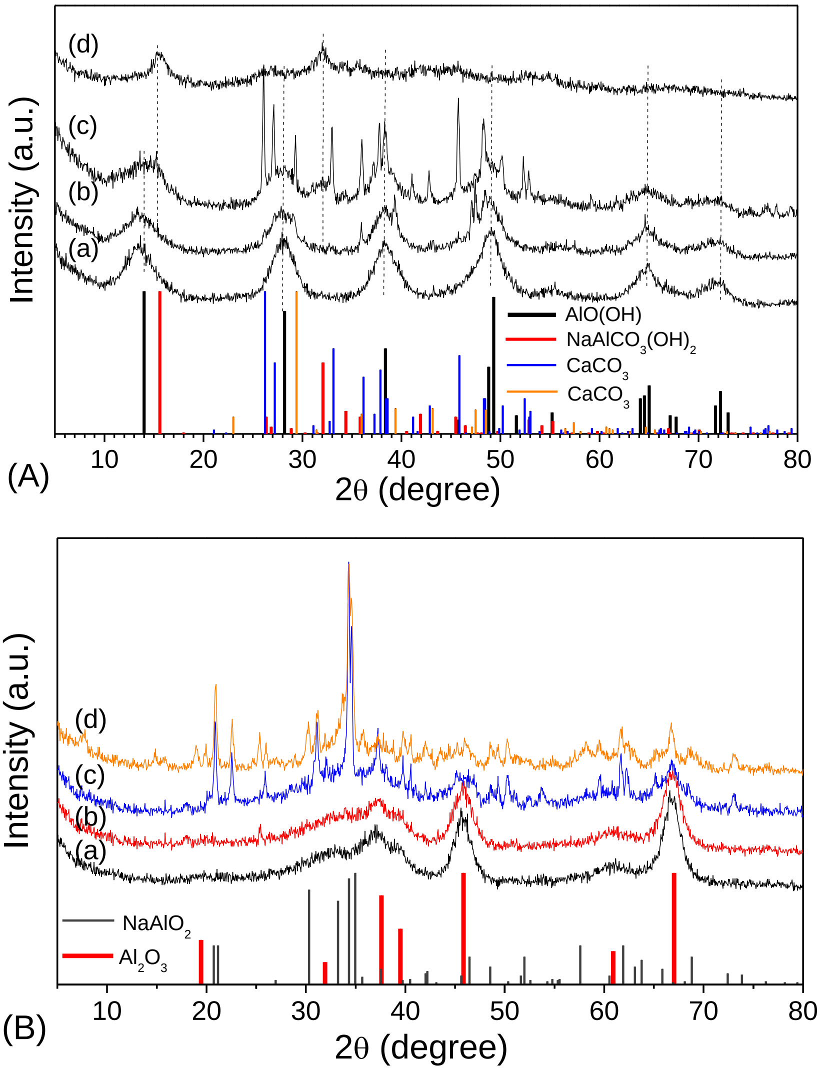

Fig. S11 XRD patterns of (A) aluminium hydroxides precursor and (B) calcined product prepared with varied alkaline solution concentrations at constant pH (9.5-10.0). (a) 1 M NaOH, (b) 0.94 M NaOH+0.06 M Na_2CO_3, (c) 0.5 M NaOH+0.5 M Na_2CO_3, (d) 1 M Na_2CO_3. AlOOH (pseudoboehmite, JCPDS 49-0133), $NaAlCO_3(OH)_2$ (Dawsonite, JCPDS 45-1359), Al_2O_3 (JCPDS 10-0425), $NaAlO_2$ (JSPDS, 33-1200).

For the precursor, the peaks match well with AlO(OH) (pseudoboehmite, JCPDS 49-0133) with major peaks at 2θ=14.0°, 28.2°, 38.4°, 48.8°, 49.3°, 64.1°, 64.5°, 65.0°, 71.7°, 72.2°. At high concentration of [Na_2CO_3], the peaks of AlO(OH) become weak and crystalline phase of $NaAlCO_3(OH)_2$ (Dawsonite, JCPDS 45-1359) can be observed, and become evident using pure Na_2CO_3 as precipitant. For the sample prepared with 0.5 M NaOH+0.5 M Na_2CO_3, some peaks are assigned to $CaCO_3$ (Aragonite, blue vertical line, JCPDS 41-1475, and calcite, vertical orange line, JCPDS 05-0586), due to contamination of Ca^{2+} during washing of this sample using laboratory water since reverse osmosis water was not available. Nevertheless, the patterns do confirm the existence of $NaAlCO_3(OH)_2$, when was Na_2CO_3 used as a precipitating agent.

After calcination at 950°C for 5 h, the pseudoboehmite AlO(OH) transformed to Al_2O_3. However, accurate assignment of the XRD pattern is not certain as the peaks match well with several types of Al_2O_3 (JCPDS 50-0741 and JCPDS 10-0425 as shown in the figure, a type of Al_2O_3 with slow transition to α-Al_2O_3 at 1000°C, or θ-Al_2O_3, JCPDS 23-1009). The $NaAlCO_3(OH)_2$ phase transformed to $NaAlO_2$ after decomposition at high temperature. The peaks match well with $NaAlO_2$ (JSPDS, 33-1200).

2.10 Characterisation of precursor and calcined material with Cu:Al = 3:1 (Fig. S12)

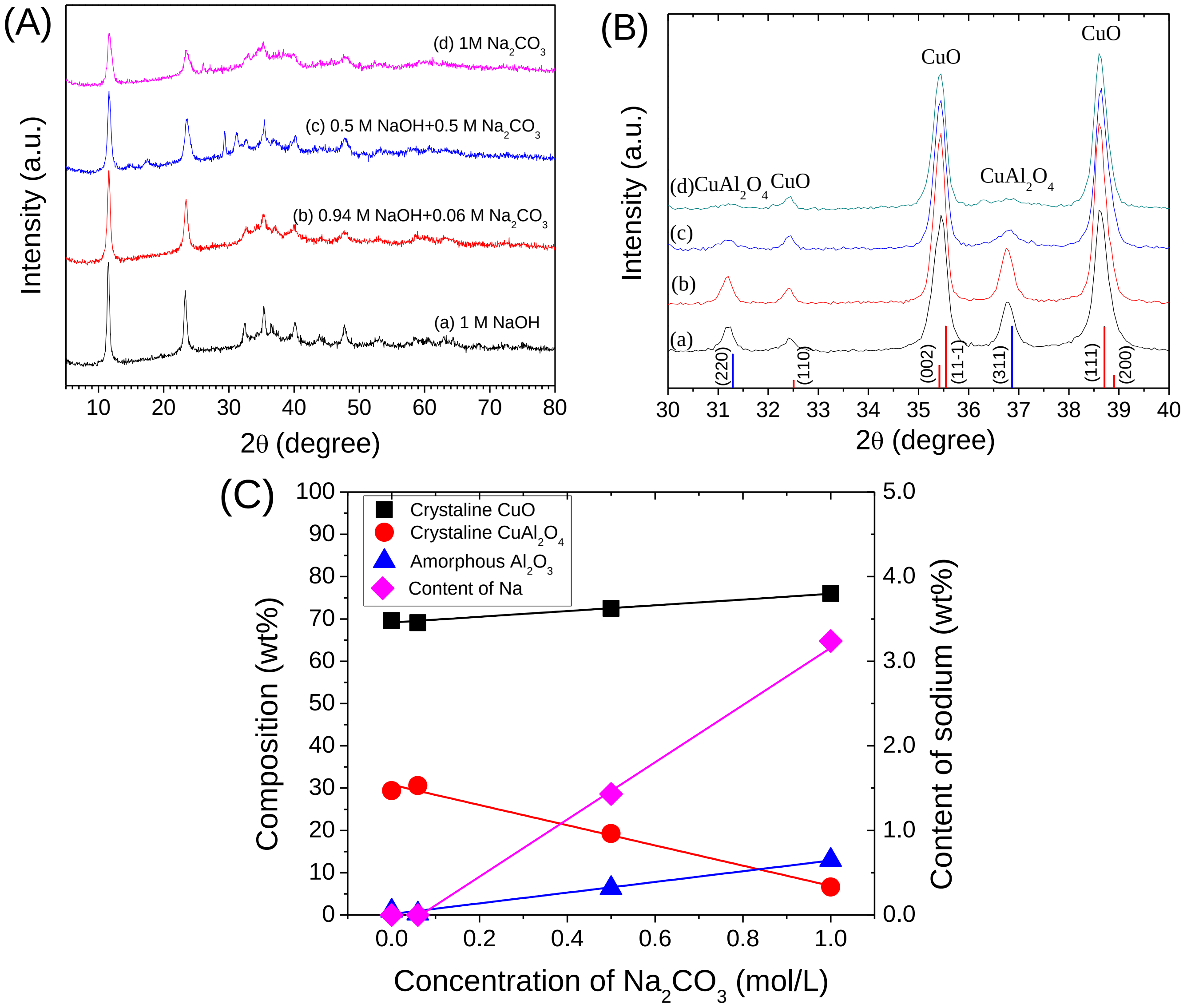

Fig. S12 XRD patterns of Cu-Al LDH precursor prepared with Cu^{2+}:Al^{3+}=3:1 with varied alkaline precipitant and derived CuO/Al_2O_3 nanocomposite. (A) Precursor with the alkaline solution concentration marked. (B) Derived CuO/Al_2O_3 nanocomposite with (a) 1 M NaOH, (b) 0.94 M NaOH+0.06 M Na_2CO_3, (c) 0.5 M NaOH+0.5 M Na_2CO_3, (d) 1 M Na_2CO_3. The crystalline patterns correspond to CuO (Tenorite, JCPDS 45-1548, vertical red lines) and $CuAl_2O_4$ (JCPDS 33-0448, vertical blue lines), respectively. (C) Correlation of the composition of calcined product, residual content of sodium with the concentration of Na_2CO_3 in the alkaline precipitating agent. The lines are added to guide the eyes.

2.11 Summary of physical and chemical properties (Table S1)

Table S1 Summary of physical and chemical properties of LDH precursor and derived CuO/Al_2O_3 nanocomposite.

(a) Molar ratio of Cu^{2+} to Al^{3+} is varied, $[Cu^{2+}]+[Al^{3+}]=1$ M, using a precipitant consisting of a mixture of NaOH and Na_2CO_3 (0.5 M of each).

$[Cu^{2+}]:[Al^{3+}]$	Precursor		Derived mixed metal oxides						
	d(003) (Å)	$L_{(LDH)}$ [a] (nm)	L_{CuO} [a] (nm)	$L_{CuAl2O4}$ [a] (nm)	CuO [b] (wt%)	$CuAl_2O_4$ [b] (wt%)	Al_2O_3 [b] (wt%)	x_{CuO} [c] (wt%)	R_O [d] (wt%)
Cu:Al=1:0	-	-	35.2±1.1	-	100	0	0	100	20
Cu:Al=3:1	7.61	13.8	40.7±3.8	20.4±5.1	72.5	19.3	6.3	82.5	16.5
Cu:Al=2	7.57	20.1	52.1±7.1	28.8±10.3	60.7	32.7	6.6	75	15
Cu:Al=1.5:1	7.63	22.3	36.0±2.0	17.5±1.5	50.1	45.5	4.4	70	14
Cu:Al=1:1	7.62	39.8	25.5±0.7	11.6±0.4	43.1	38.5	18.3	60	12
Cu:Al=1:2	7.60	29.2	22.4±1.1	12.3±0.4	11.8	73.6	14.7	44	8.8
Cu:Al=1:6	-	-	-	6.5±6.3	0.5	44.5	55.0	20	4

(b) $[Cu^{2+}]:[Al^{3+}]=3:1$, with precipitating agent varied, $[NaOH]+[Na_2CO_3]=1$ M. The nominal loading of CuO is 82.5 wt%.

$[NaOH^-]:[Na_2CO_3]$	Precursor		Derived mixed metal oxides							
	d(003) (Å)	$L_{(LDH)}$ [a] (nm)	L_{CuO} [a] (nm)	$L_{CuAl2O4}$ [a] (nm)	CuO [e] (wt%)	$CuAl_2O_4$ [e] (wt%)	Al_2O_3 [e] (wt%)	Na_2O [e] (wt%)	Na [e] (wt%)	R_O [d] (wt%)
1 M:0 M	7.70	20.3	35.2±3.1	41.2±7.6	69.62	29.41	0.97	0.0	0	16.5
0.94 M:0.06 M	7.64	16.0	47.0±4.8	39.1±6.2	69.09	30.61	0.30	0.0	0	16.5
0.5 M:0.5 M	7.61	13.8	40.7±3.8	20.4±5.1	72.47	19.26	6.34	1.93	1.43	16.5
0 M:1 M	7.59	11.0	39.0±3.5	28.5±11.8	76.00	6.61	13.02	4.37	3.24	16.5

[a] $L_{(LDH)}$, L_{CuO}, $L_{CuAl2O4}$, crystallite size of LDH precursor d(003), CuO d(11-1) and (111), and $CuAl_2O_4$ d(311), in the calcined product, respectively. The data was calculated using the Scherrer equation, respectively.

[b] Quantitative content calculated from the relative ratio of CuO to $CuAl_2O_4$ in XRD and mass balance.

[c] Nominal loading of CuO (wt%)

[d] The oxygen storage capacity (R_O) is the overall amount of reducible oxygen, calculated from the nominal loading.

[e] Quantitative content as measured from elemental analyses by ICP-AES.

2.12 SEM of precursor and calcined product with typical Cu-Al ratios (Fig. S13)

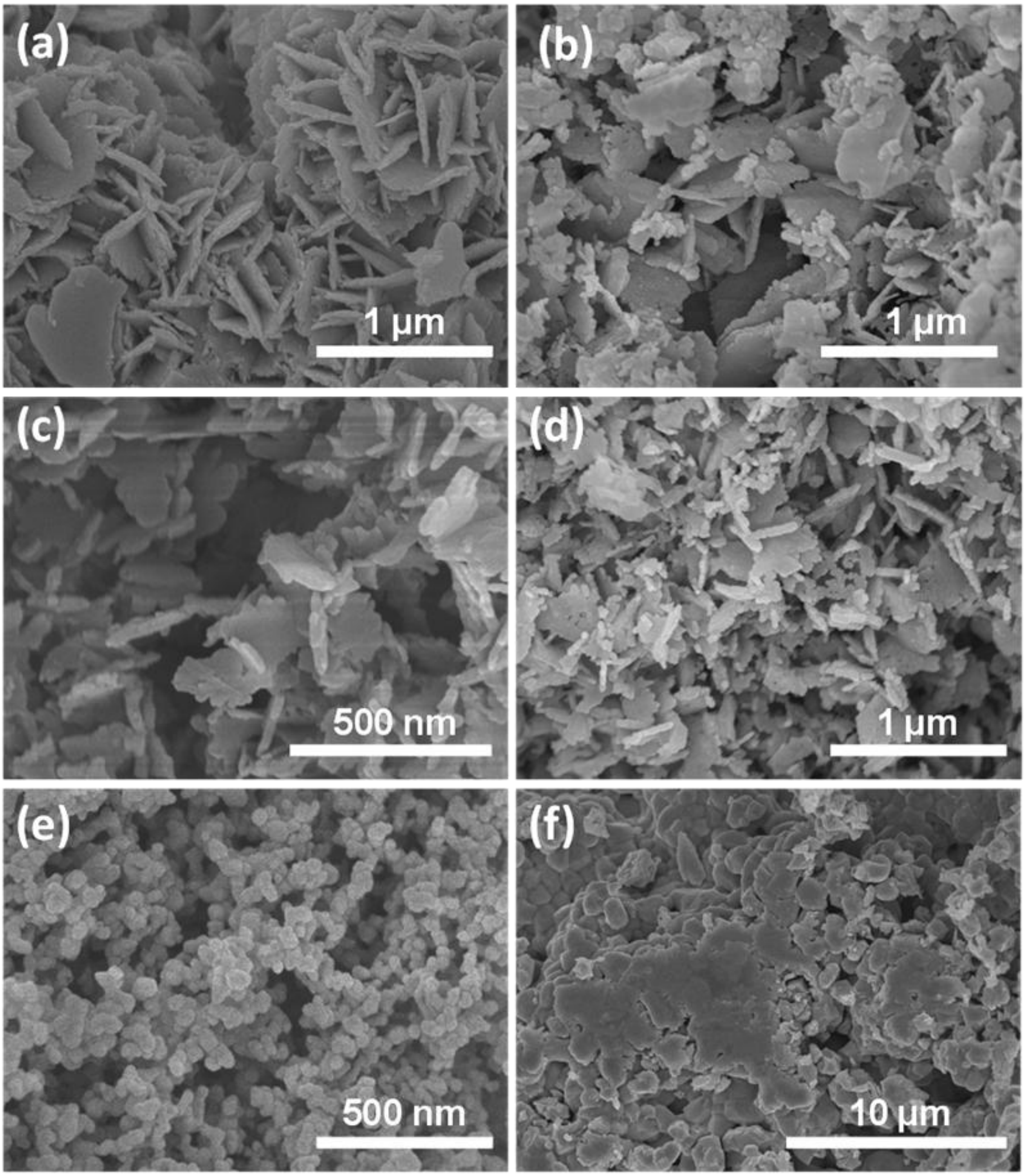

Fig. S13 SEM images of precursor and derived metal oxides. (a) Cu-Al-LDH, Cu:Al=1:1, precipitated by mixture of NaOH and Na_2CO_3 (1 M of each) and (b) derived 60 wt% CuO/Al_2O_3, (c) Cu-Al-LDH, Cu:Al=3:1 precipitated by mixture of NaOH and Na_2CO_3 (0.5 M of each) and (d) derived 82.5 wt% CuO/Al_2O_3, (e) Precursor with Cu:Al=1:0 precipitated by mixture of NaOH and Na_2CO_3 (0.5 M of each), and (f) as calcined 100 wt% CuO.

The aluminium-free copper-based precipitate consisted of amorphous spherical-like particles (~50 nm), with very weak XRD peaks corresponding to rouaite $Cu_2(OH)_3NO_3$. Upon calcination at 950°C the sintering of CuO lead to the formation of micrometer-sized grains as indicated by sharp peaks in the XRD pattern.

3. Oxygen storage capacity and gaseous O_2 release capacity

3.1 TPR of oxygen storage materials with representative loadings of CuO (Fig. S14)

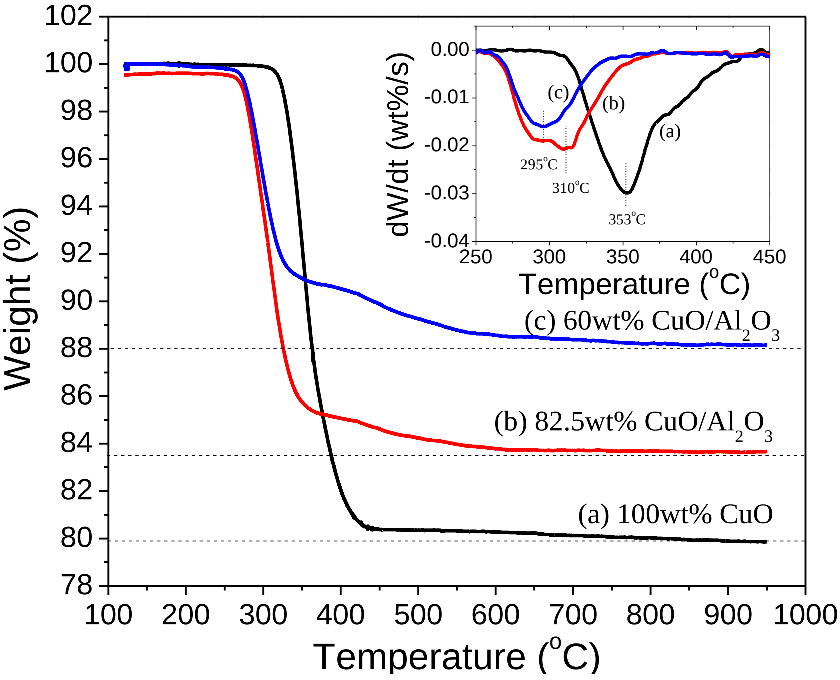

Fig. S14 TGA profiles of H_2-TPR reduction of CuO/Al_2O_3 with loading marked. The derivative is shown in the inset. (a-b) Precipitating agent was mixture of NaOH and Na_2CO_3, 0.5 M each. (c) Precipitating agent was mixture of NaOH and Na_2CO_3 (1 M of each). The horizontal dashed lines indicate the final weight according to the nominal loading.

3.2 TPR of oxygen storage materials prepared with various precipitating agent (Fig. S15)

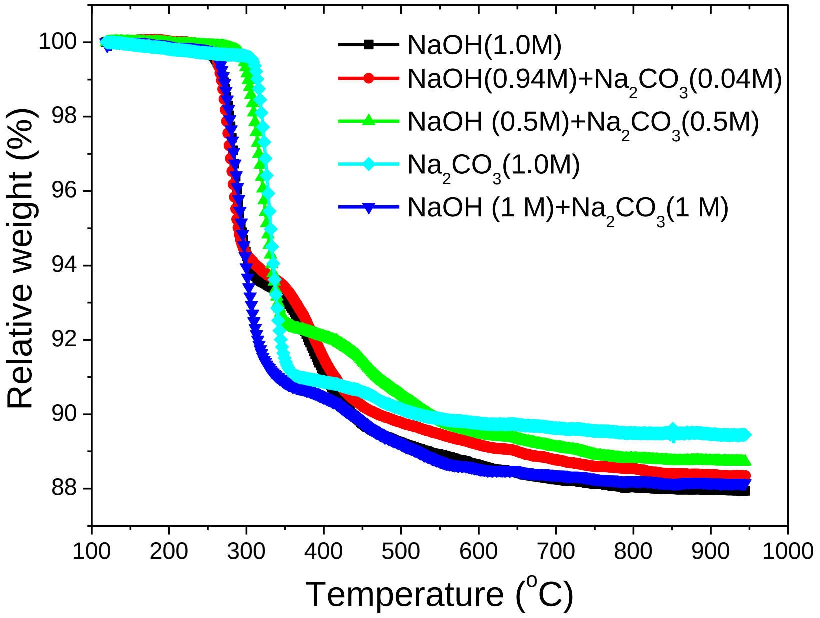

Fig. S15 TPR profiles of reduction of Cu-based oxygen carriers with nominal CuO loading of 60 wt% prepared from various precipitants. (a)1 M NaOH, (b) 0.94 M NaOH+0.06 M Na_2CO_3, (c) 0.5 M NaOH+ 0.5 M Na_2CO_3, (d) 1 M NaOH+ 1 M Na_2CO_3, (e) 1 M Na_2CO_3.

3.3 Gaseous oxygen release during decomposition in TGA (Fig. S16)

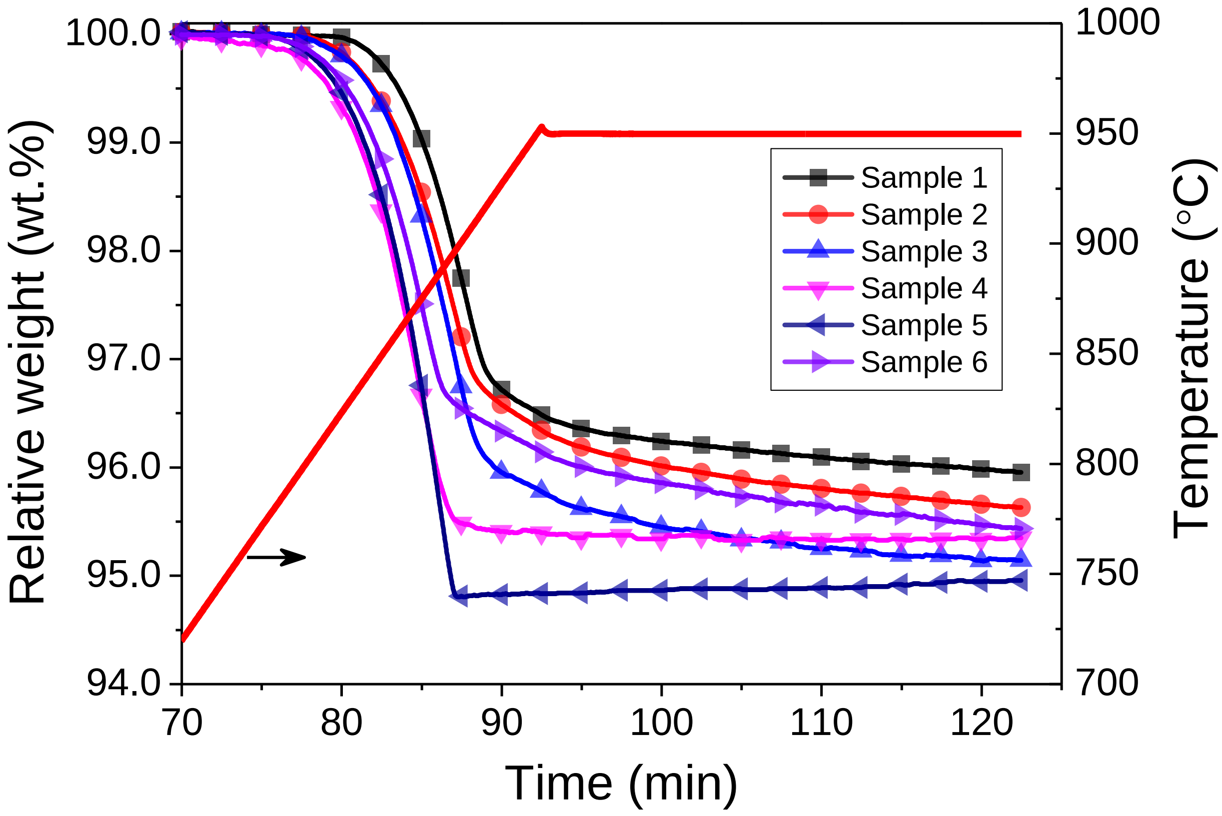

Fig. S16. Temperature programmed decomposition of Cu-based oxygen carrier as calcined from Cu-Al LDH precursors. A batch of particles of each sample (~10 mg) were heated to 950 °C at 10°C/min, then kept at 950°C for 30 min. The samples were prepared from calcination of Cu-Al LDH precursors, with varied precipitant at constant pH of 9.6±0.1. The precipitants were: (1) 1 M NaOH, (2) mixture of 0.96 M NaOH and 0.04 M Na_2CO_3, (3) 0.5 M NaOH+ 0.5 Na_2CO_3, (4) 1 M Na_2CO_3, (5) 1 M NaOH+1 M Na_2CO_3, and (6) increasing pH method.

For samples (3-5), we observed weight loss below 700°C due to absorption of CO_2 and H_2O, which is attributed to the memory effect of LDHs. All the TGA data were normalized from the stable point at about 700°C, after which the weight became stable and gaseous O_2 release started.

In principle, the $CuAl_2O_4$ should be able to release O_2. However, here we demonstrate that the samples containing more $CuAl_2O_4$ gave much slower rates of O_2 release, and the decompositions were not complete over the isothermal stage at 950°C for 30 min. In contrast, sample 5 with smaller CuO crystals (~30 nm) dispersed in amorphous nanoplatelet-like mesoporous support, showed only one fast state of weight loss up to 5 wt%, corresponding well to the mass balance. In practical reactions, fast cyclic reduction and oxidation of oxygen carrier will be performed by circulating between two reactors, therefore the slow kinetics of O_2 release from $CuAl_2O_4$ is not favourable and essentially does not contribute to the gaseous O_2 release. Here we define the weight loss of the fast stage as the measured O_2 release capacity, that is, the O_2 released by crystalline CuO. The data are listed in Table 1 in the main text. The data agree very well with the mass balance derived from elemental analysis and crystalline phase analysis.

4. CLOU cycles

4.1 CLOU cycles with partial and complete oxygen release at 900°C (Fig. S17)

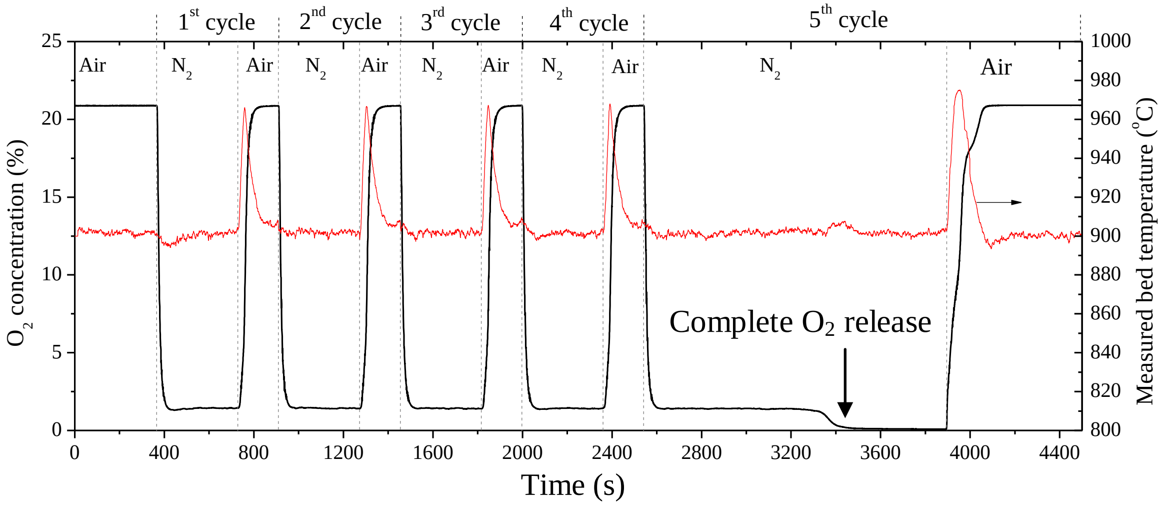

Fig. S17 Representative profile of oxygen release and uptake of 15 g of 60 wt% CuO/Al_2O_3 at set-point temperature of 900 °C. Vertical dashed lines indicate the switching of inlet gases of N_2 (50.0 cm^3/s, STP) during decomposition and air (47.4 cm^3/s, STP) during oxidation. The Cu-based mixed metal oxides with nominal CuO loading of 60 wt% was calcined from Cu-Al LDH, with $Cu^{2+}:Al^{3+}=1:1$ total concentration of 2 M, precipitated with a mixture of NaOH and Na_2CO_3 (1 M of each). The content of sodium in the fresh 60wt% CuO/Al_2O_3 was 7.9 wt%, as measured by ICP-AES.

Here we show the representative cycles of uptake and release of oxygen from 15 g (as measured in the fully oxidised state) of co-precipitated CuO/Al_2O_3 fluidised at the set-point temperature of 900°C. The fluidising gas during oxidation was air: during decomposition it was pure N_2. It can be seen that as soon as the fluidising gas was switched from air to N_2, the oxygen concentration in the off-gases decreased rapidly and then stabilised at a level of 1.41 vol%, close to the equilibrium value of 1.51 vol% at 900°C. In the first 4 cycles, the period in N_2 was too short to give complete decomposition, and the $[O_2]$ remained close to the equilibrium value. In contrast, for the fifth cycle, $[O_2]$ was stable for nearly 900 s, and then decreased to zero (close to measurement limit), suggesting that all the oxygen carrier had decomposed fully to Cu_2O, as verified by XRD analysis.

In these experiments, the enthalpy of decomposition of CuO to Cu_2O (ΔH^0_{1223K}= +261.1 kJ/mol O_2) is significant, leading to significant excursions in measured temperature for a given set point, as seen in Fig. S18. However, it should be noted that the temperature varied during the dynamic O_2 release process. It is important to distinguish between set point of the temperature controller (T_{sp}) and the measured temperature of the bed (T_b), which may differ from the particle temperature (T_P). At the beginning of each cycle, the temperature of the bed is stable and equal to T_{sp}; during each cycle T_b varies as the controller attempts to compensate for heat absorbed and given out by the decomposition and oxidation, respectively.

As noted in the main text, in certain cycles, after complete release of the oxygen, a small fraction of the bed material (about 200 mg) was sampled from the reactor through a quartz sampling tube connected to a vacuum pump, for *ex situ* analysis and the same amount of fresh particles (200 mg) was added to the bed. The overall performance of the particles did not vary after each sampling and make-up process. Over the duration of 121 cycles, a total of 1.0 g of reacted particles was sampled and 1.0 g of fresh material was added to the bed. The major contributor to the uncertainties in mass balance was the uncertainty associated with the flow rate of N_2, which is around ±5% of the recorded flowrate. After the cycling experiment, the mass of the bed recovered at the end of the cycling experiment was around 14.6 g, which is 97 wt% of the original mass of 15.0 g, giving a rough estimate of elutriation rate of 0.067 wt%/h. Among the 14.6 g of recovered particles, 14.0 g of the sample remained in the same size fraction as fresh particles, and the other 0.6 g were finer ($d_p < 500$ µm). Thus the average attrition rate of 0.17 wt%/h was estimated, ignoring the effect of the addition of fresh particles after solid sampling, which may increase or decrease the rate of elutriation, depending on the evolution of the mechanical strength of the particles over cycling.

4.2 Long-term multiple cycles of oxygen release and storage at 950°C (Fig. S18)

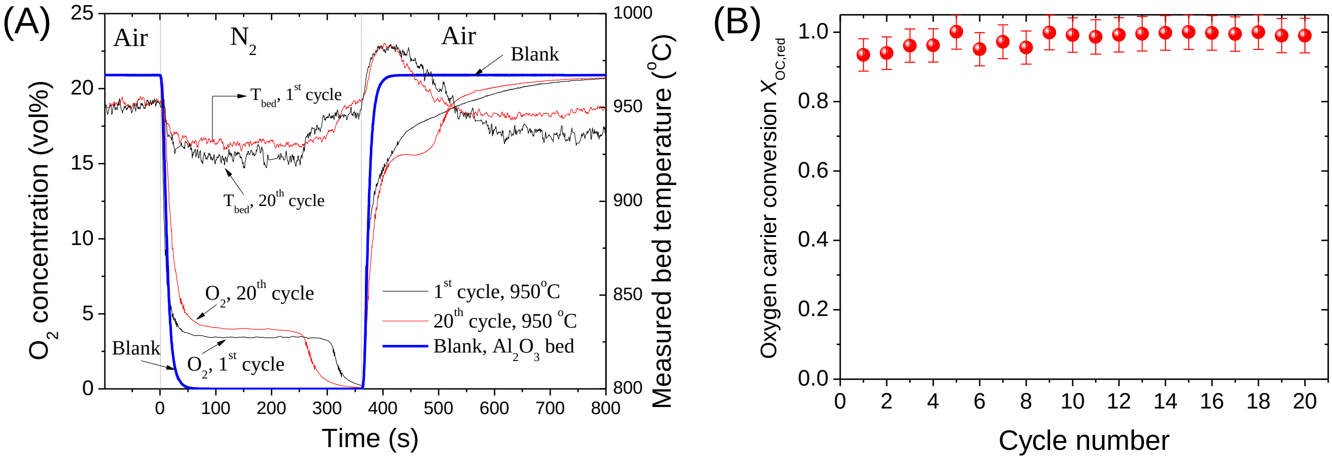

Fig. S18 (a) O_2 concentration and measured bed temperature profiles of cyclic O_2 release and storage of 60wt% CuO/Al_2O_3 oxygen carrier at the 1st and 20th cycle at 950°C in a fluidised bed. The vertical dashed line indicates the switch between N_2 and air. The inlet fluidising gas was switched between N_2 (50.0 cm^3/s, STP) during decomposition and air (47.4 cm^3/s, STP) during oxidation, as indicated by the vertical dashed lines. (b) Overall oxygen carrier conversion as a function of number of cycles at 950°C. The 60 wt% CuO/Al_2O_3 was calcined from Cu-Al LDH, with $Cu^{2+}:Al^{3+}=1:1$ total concentration of 2 M, precipitated with a mixture of NaOH and Na_2CO_3 (1 M of each). The content of sodium in the fresh 60wt% CuO/Al_2O_3 was 7.9 wt%, as measured by ICP-AES.

4.3 Effect of temperature on O_2 release (Fig. S19)

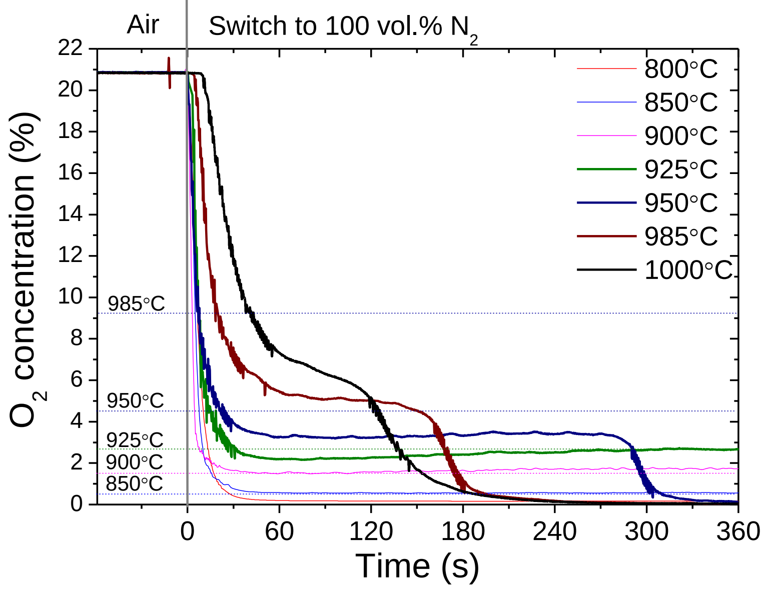

Fig. S19 Concentration profiles of oxygen release of 60% CuO/Al_2O_3 oxygen carrier at nominal operating temperature. The horizontal dashed lines are equilibrium partial pressure of O_2 based on CuO/Cu_2O couple, calculated from the nominal temperature, as marked above the lines. The Cu-based mixed metal oxides with nominal CuO loading of 60 wt% was calcined from Cu-Al LDH, with $Cu^{2+}:Al^{3+}=1:1$ total concentration of 2 M, precipitated with a mixture of NaOH and Na_2CO_3 (1 M of each). The content of sodium in the fresh 60wt% CuO/Al_2O_3 was 7.9 wt%, as measured by ICP-AES.

At lower temperatures, 800-925°C, the oxygen concentration reaches a stable value, which is close to the expected equilibrium value, indicating that the intrinsic chemical rate of reaction is high, and that in these experiments the observed rate is sufficiently rapid to establish a concentration of oxygen close to equilibrium in the fluidised bed. At temperatures >925°C, the equilibrium partial pressure, and hence the rate of decomposition, is sufficiently high for there to be significant changes in the temperature of the fluidised bed owing to the endothermic decomposition. The measured O_2 partial pressure was much lower than equilibrium value for the nominal temperature of the reactor, but in line with the instantaneous equilibrium pressure which would be expected from the temperature of the bed.

4.4 O_2 release capacity of fresh and used oxygen carrier material (Fig. S20)

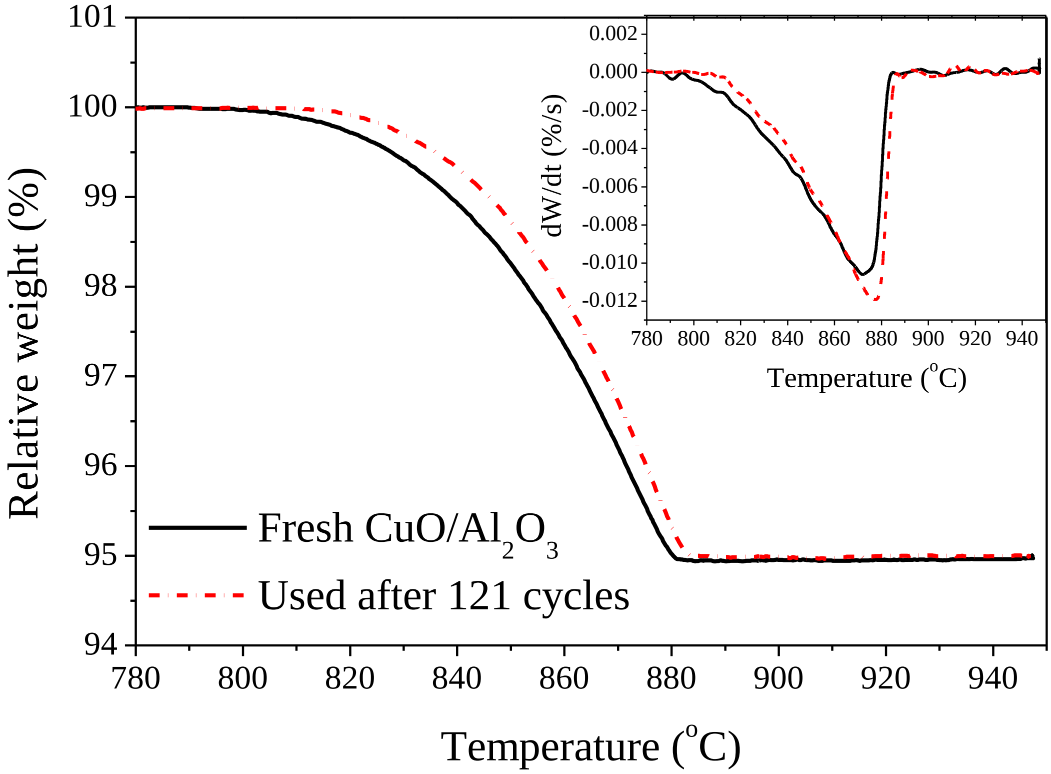

Fig. S20 Temperature programmed decomposition of fresh and used 60 wt% CuO/Al_2O_3 exposed to 121 consecutive oxygen release and storage cycles. The Cu-based mixed metal oxides with nominal CuO loading of 60 wt% was calcined from Cu-Al LDH, with Cu^{2+}:Al^{3+}=1:1 total concentration of 2 M, precipitated with a mixture of NaOH and Na_2CO_3 (1 M of each). The content of sodium in the fresh 60wt% CuO/Al_2O_3 was 7.9 wt%, as measured by ICP-AES.

Ex situ temperature programmed decomposition was performed to evaluate the capacity of gaseous O_2 release. The capacity for oxygen release and storage is stable with the overall weight loss constant at ~5wt%. This oxygen uncoupling capacity is somewhat lower than that estimated from the TPR results, which may be due to the formation of trace amount of $CuAl_2O_4$ which is reducible but does not release oxygen over the temperature range in the test. The oxygen release capacity (CuO to Cu_2O) of the used oxygen carrier after 121 cycles at 900°C is almost the same as that of the fresh material.

4.5 Oxygen storage capacity of fresh and used oxygen carrier material by H_2-TPR in TGA (Fig. S21)

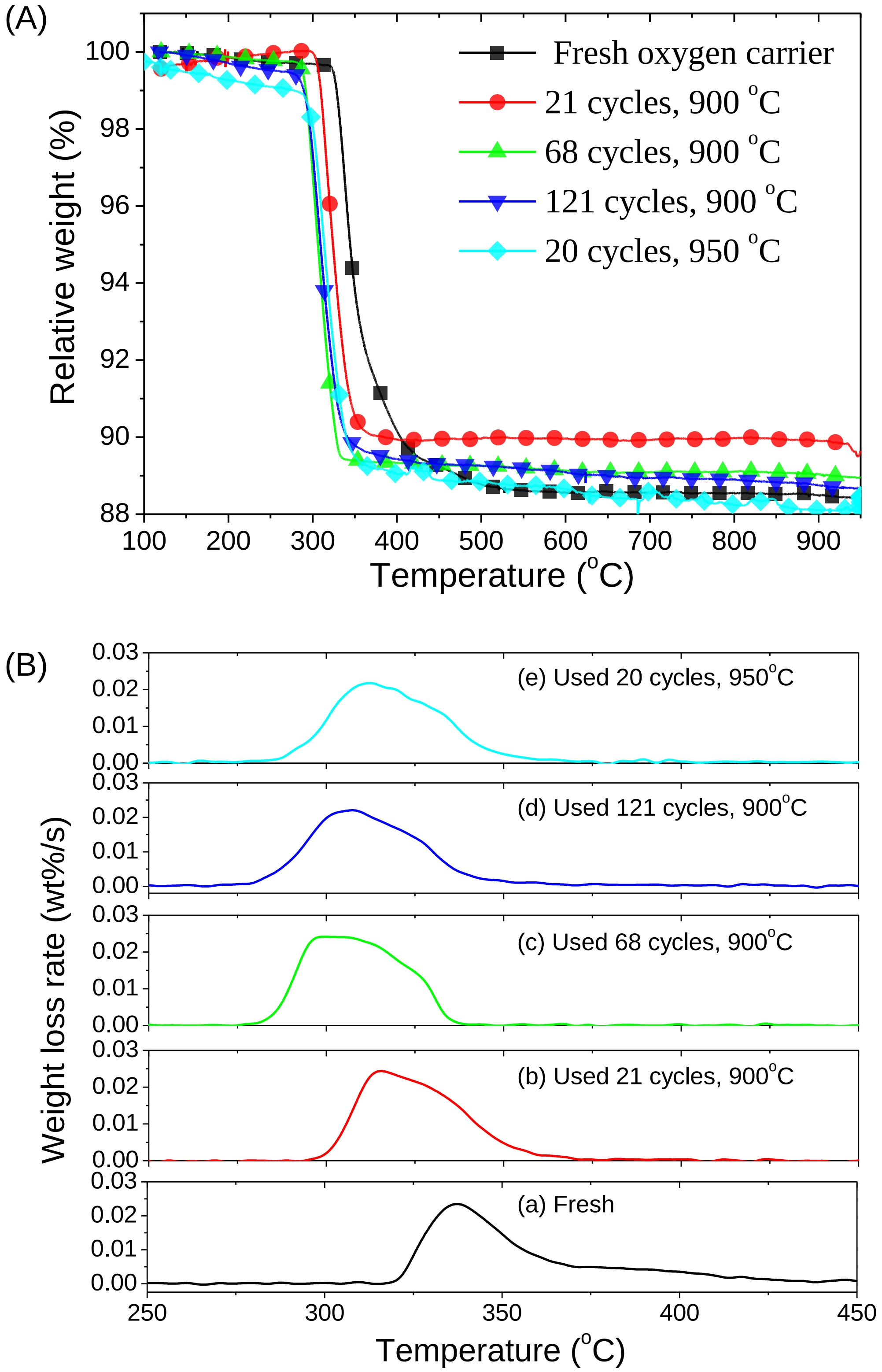

Fig. S21 Temperature programmed reduction of fresh and used oxygen carrier sampled in the CLOU experiments. The Cu-based mixed metal oxides with nominal CuO loading of 60 wt% was calcined from Cu-Al LDH, with Cu^{2+}:Al^{3+}=1:1 total concentration of 2 M, precipitated with a mixture of NaOH and Na_2CO_3 (1 M of each). The content of sodium in the fresh 60wt% CuO/Al_2O_3 was 7.9 wt%, as measured by ICP-AES.

4.6 XRD patterns of oxygen carrier materials (Fig. S22)

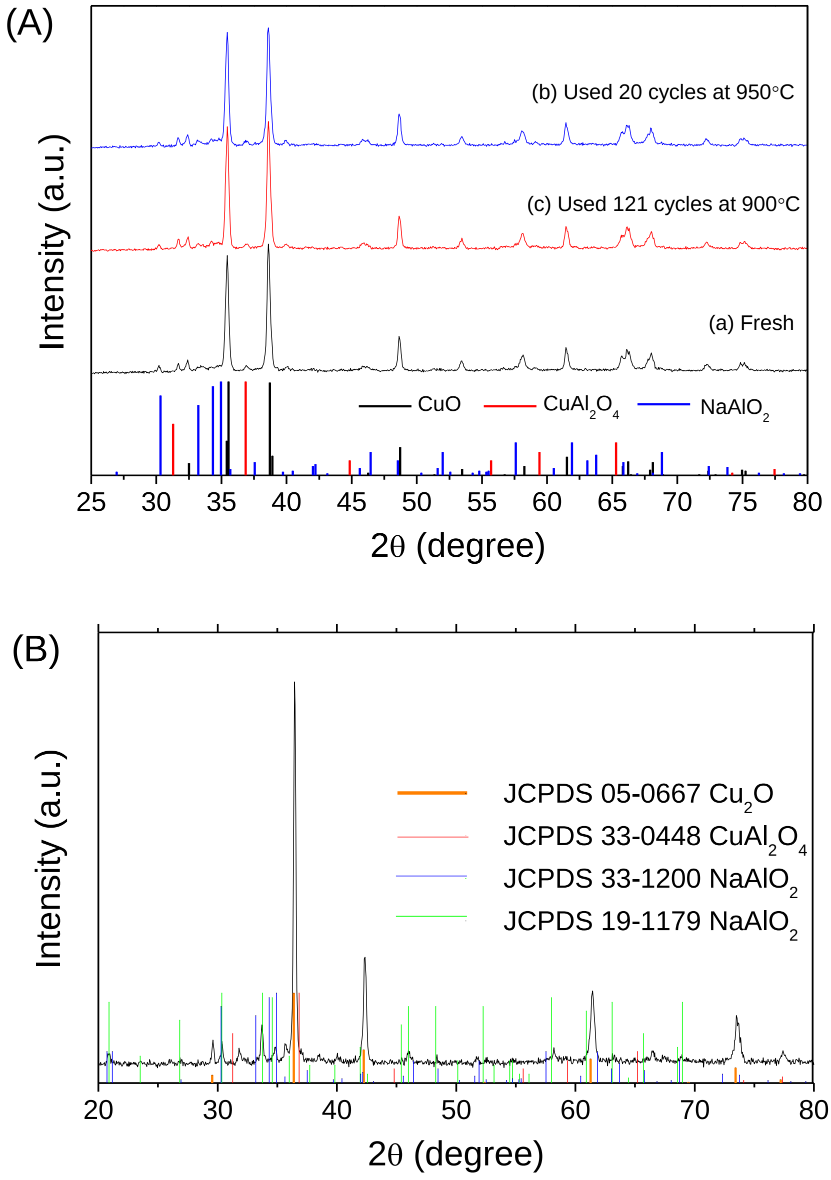

Fig. S22 (A) XRD pattern of fresh and used co-precipitated oxygen carrier with 60 wt% CuO/Al_2O_3. (a) fresh particles calcined at 950°C for 5 h, (b) samples extracted after 121 cycles, (c) samples recovered after 20 cycles at 950°C, (d) sample used after 50 cycles of decomposition/oxidation at 700-1000°C, (B) sample completely decomposed in N_2 at 900 °C. Spinel copper aluminate $CuAl_2O_4$ (JCPDS 33-0448); $CuAlO_2$ (JCPDS 40-1037); $NaAlO_2$ (JCPDS 33-1200); CuO (JCPDS 48-1548); Cu_2O (JCPDS 05-0667). The Cu-based mixed metal oxides with nominal CuO loading of 60 wt% was calcined from Cu-Al LDH, with Cu^{2+}:Al^{3+}=1:1, total concentration of 2 M, precipitated with a mixture of NaOH and Na_2CO_3 (1 M of each). The content of sodium in the fresh 60wt% CuO/Al_2O_3 was 7.9 wt%, as measured by ICP-AES.

The major crystalline phase CuO is maintained over the long-term oxygen uncoupling cycles. The amorphous Al_2O_3 support was stable and did not transform to other crystallised Al_2O_3 phases. The other minor phase such as $NaAlO_2$ is also very stable over the cyclic operation. The lattice constants for the crystals of different phases were calculated using Bragg's law and the thickness of crystallite, or the crystallite size, with the Scherrer equation. The average crystallite size of CuO in the sample exposed to multiple cycles at 900 and 950°C CuO were approximate equal to that of the fresh oxygen carrier (~35 nm). The Al_2O_3 still behaved as X-ray amorphous and there we no evident peaks of copper aluminate.

4.7 SEM images of used 60 wt% CuO/Al_2O_3 after multiple CLOU cycles (Fig. S23)

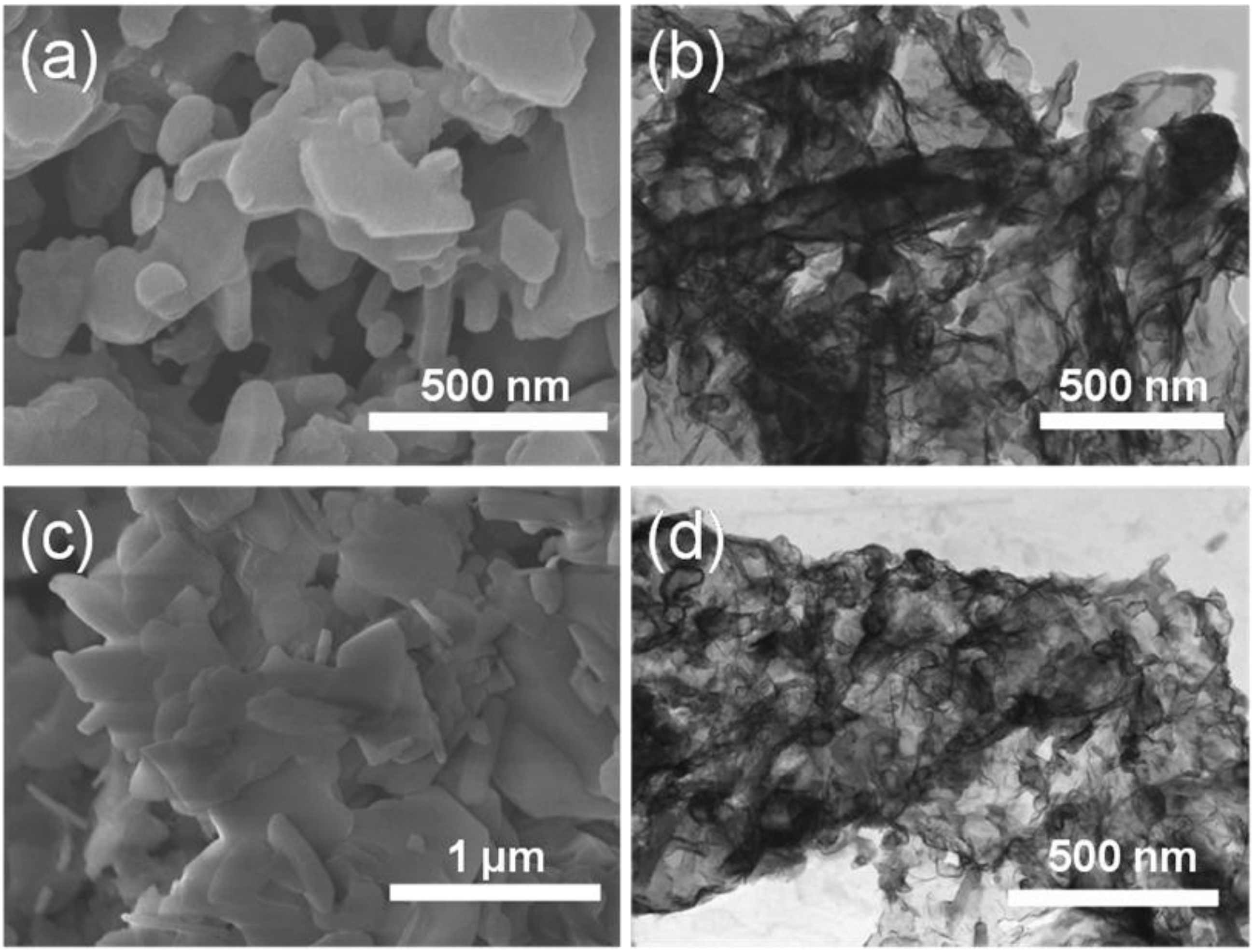

Fig. S23 Representative SEM and STEM images of cross-section of CuO/Al_2O_3 particles with nominal loading of 60 wt%. (a-b) after 121 cycles of oxygen release and storage at 900°C, (c-d) after 20 cycles of O_2 release and storage at 950°C. Although severe sintering occurred, the interior of the particle was still mesoporous, with the nanoplatelet-like morphology observed. The STEM confirmed that the CuO crystals were still well dispersed in the support. The 60 wt% CuO/Al_2O_3 was calcined from Cu-Al LDH, with Cu^{2+}:Al^{3+}=1:1 total concentration of 2 M, precipitated with a mixture of NaOH and Na_2CO_3 (1 M of each). The content of sodium in the fresh 60wt% CuO/Al_2O_3 was 7.9 wt%, as measured by ICP-AES.

5. CLC cycles

5.1 Redox cycles of the 82.5 wt% CuO/Al_2O_3 (Fig. S24 and S25)

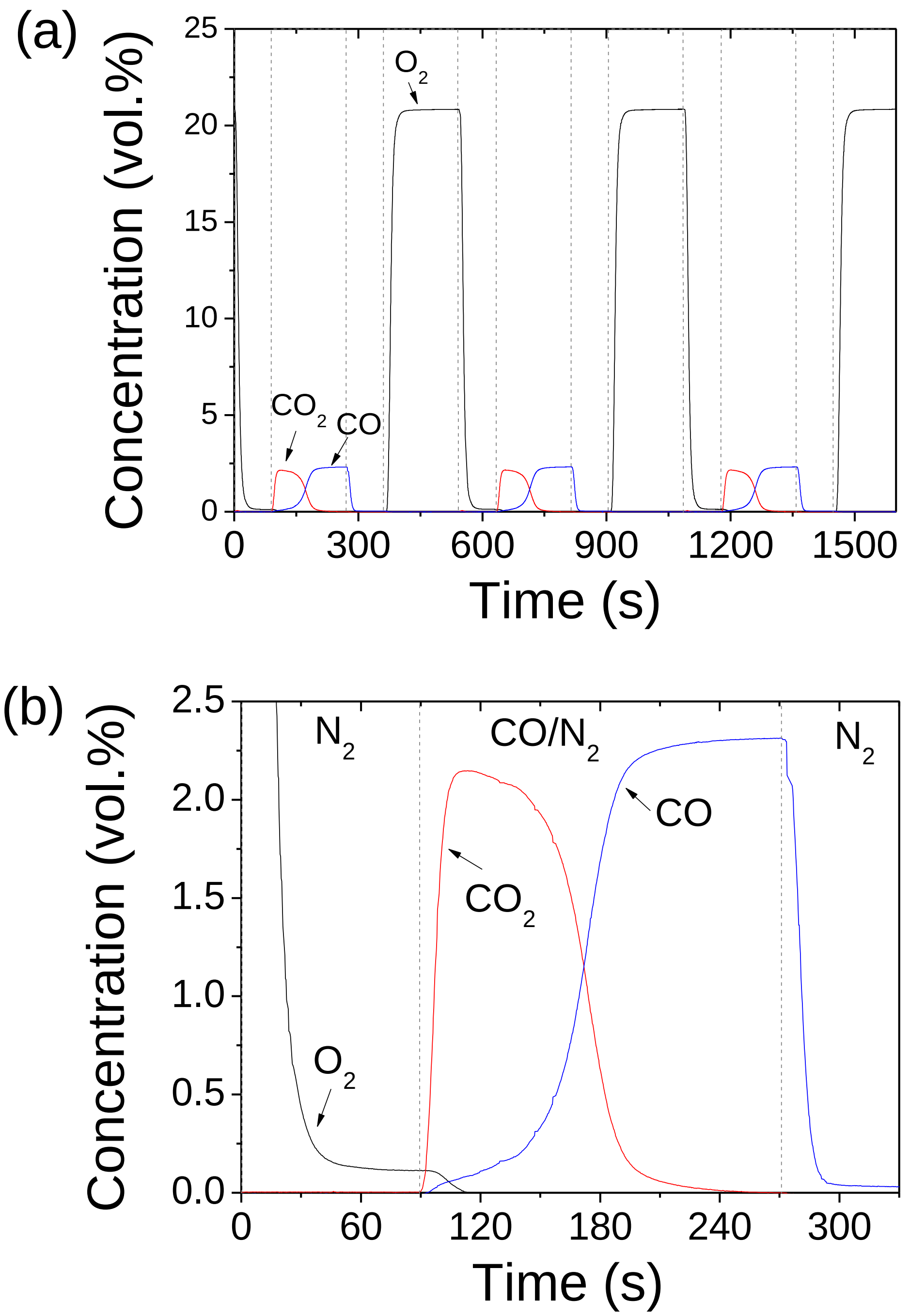

Fig. S24 Concentration profiles of (a) 0.5 g 82.5 wt% CuO/Al_2O_3 exposed to alternating reducing and oxidising conditions at typical temperature of 800 °C and (b) enlargement of the first cycle of reduction. The dashed lines denote the switch between air, ~2.4 vol.% CO/N_2 and inert N_2 purging. During the N_2 purging period prior to the reduction period, the O_2 fraction did not decrease to zero, instead it stabilised at 0.11%, very close to the equilibrium O_2 partial pressure of 0.12% at 800 °C. After the reduction and purging stage, the oxygen carrier was regenerated with air. During the initial oxidation period, no detectable CO or CO_2 was observed indicating carbon deposition during reduction was negligible. The 82.5 wt% CuO/Al_2O_3 was calcined from Cu-Al LDH, $Cu^{2+}:Al^{3+}=3:1$, total concentration of 1 M, precipitated with a mixture of NaOH and Na_2CO_3 (0.5 M of each). The content of sodium in the fresh 82.5wt% CuO/Al_2O_3 was 1.4 wt%, as measured by ICP-AES.

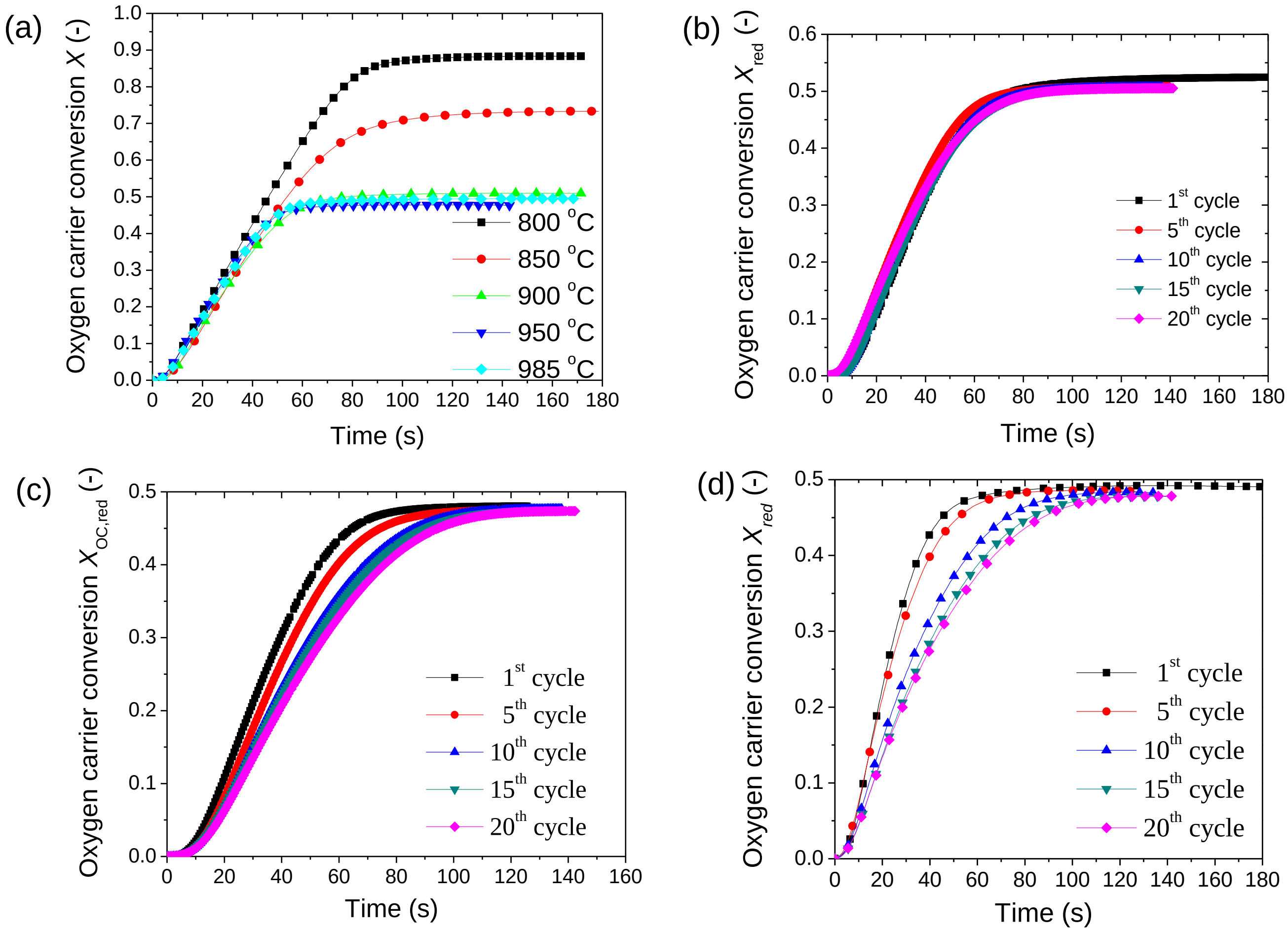

Fig. S25 Oxygen carrier conversion profiles of 82.5wt% CuO/Al_2O_3 at representative operation conditions. (a) Oxygen carrier conversion versus time at representative temperature. (b) 20 cycles at 900°C, 0.5 g, 500-710 μm, reduction: ~2.4vol.% CO in N_2, total flow rate of 65.8cm^3/s (STP). Oxidation: air, 47.4 cm^3/s (STP). (c) 20 cycles at 950°C, 0.5 g, 500-710 μm, reduction: ~2.4 vol.% CO in N_2, total flow rate of 65.8cm^3/s(STP). Oxidation: 10vol.% O_2 in N_2, total flow rate of 47.4 cm^3/s (STP). (d) 20 cycles at 985°C, 0.25 g, 500-710 μm, reduction: ~2.4vol.% CO in N_2, total flow rate of 65.8cm^3/s(STP). Oxidation: air, 47.4 cm^3/s(STP). The 82.5 wt% CuO/Al_2O_3 was calcined from Cu-Al LDH, Cu^{2+}:Al^{3+}=3:1, total concentration of 1 M, precipitated with a mixture of NaOH and Na_2CO_3 (0.5 M of each). The content of sodium in the fresh 82.5wt% CuO/Al_2O_3 was 1.4 wt%, as measured by ICP-AES.

On the first cycle, the initial rate of reaction is largely limited by external mass transfer, resulting in little change in rate with temperature (as seen in (a)). At high loading of CuO of 82.5 wt%, the oxygen carrier materials were stable over 20 redox cycles at low temperature of 800-900°C, with little change in the conversion profile (c). However, deactivation and agglomeration could occur as seen by the drop of reaction rate when they were operated at a temperature of 950°C and above (c and d). Several strategies attempted to limit the temperature during the reoxidation, and so prevent sintering. For example, the results shown in Fig S25c were obtained by reoxodising with 10 % O_2 in N_2, rather than in air as in all other experiments; whilst this did help, even in this case, there was some loss of activity of the material and agglomeration.

It should be noted that when the particles sinter and the bed agglomerates, the final solid conversion can not be the sole criterion to determine the performance of the oxygen carriers. Although all of the copper oxide could be reduced in a given amount of time, the rate of reduction decayed significantly over the 20 cycles, therefore the decrease in the final solid conversion would be inevitable if the material was cycled further. In practice, the experiment did not proceed further because it would not be sensible to operate a fluidised bed reactor with agglomerated particles.

5.2 Multiple redox cycles of 60 wt% CuO/Al_2O_3 nanocomposite (Fig. S26)

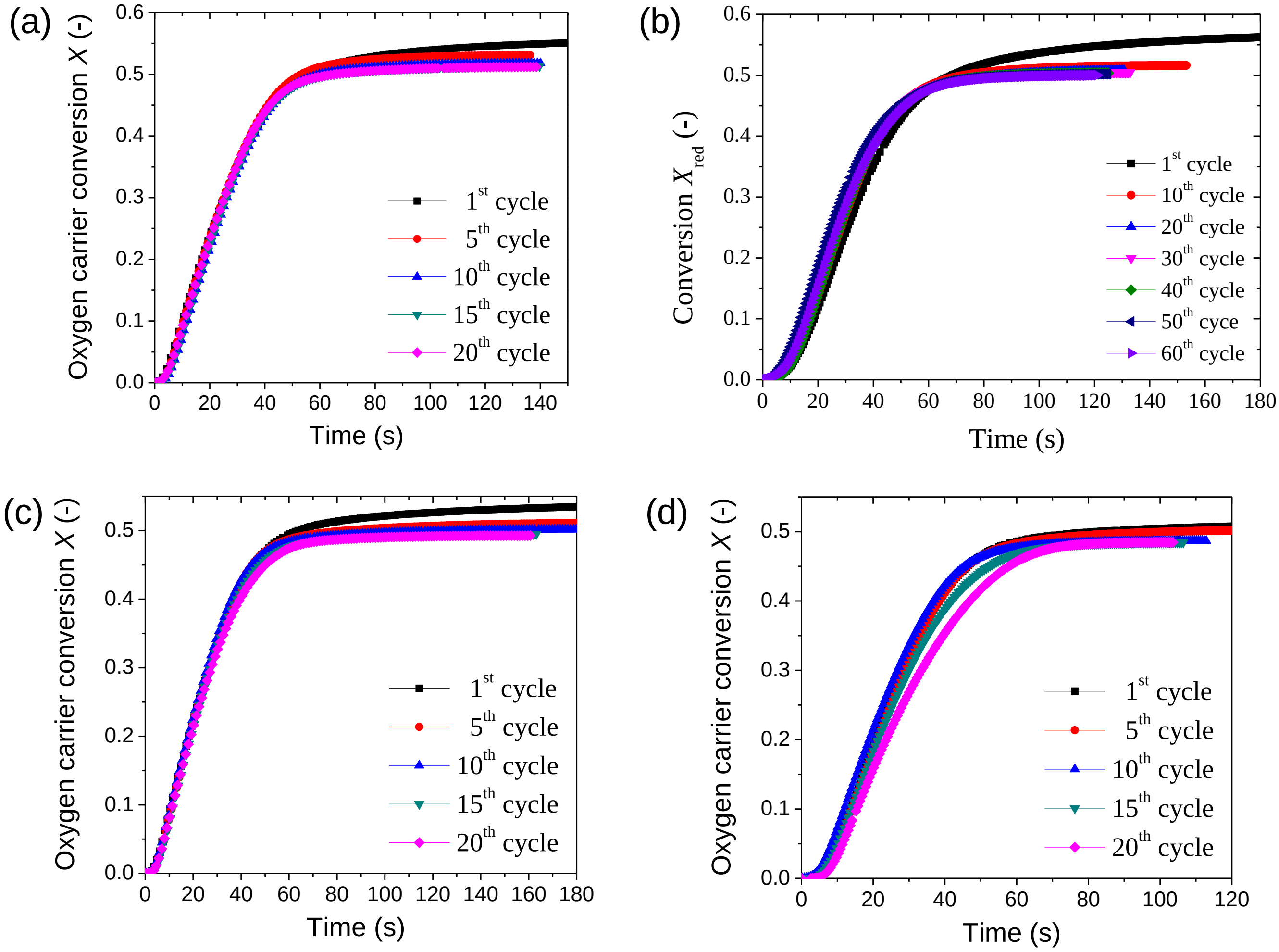

Fig. S26 CLC cycles of 60wt% CuO/Al_2O_3 at representative operation conditions. (a) 900°C, (b) 950°C, (c) 985°C, (d) 1000°C. Mass of CuO/Al_2O_3 is 0.5 g, 500-710 μm, reduction: ~2.4vol.% CO in N_2, total flow rate of 65.8cm^3/s (STP). Oxidation: air, 47.4 cm^3/s (STP). The 60 wt% CuO/Al_2O_3 was calcined from Cu-Al LDH, with Cu^{2+}:Al^{3+}=1:1 total concentration of 2 M, precipitated with a mixture of NaOH and Na_2CO_3 (1 M of each). The content of sodium in the fresh 60wt% CuO/Al_2O_3 was 7.9 wt%, as measured by ICP-AES.

5.3 SEM images of a partially sintered 82.5 wt% CuO/Al_2O_3 (Fig. S27)

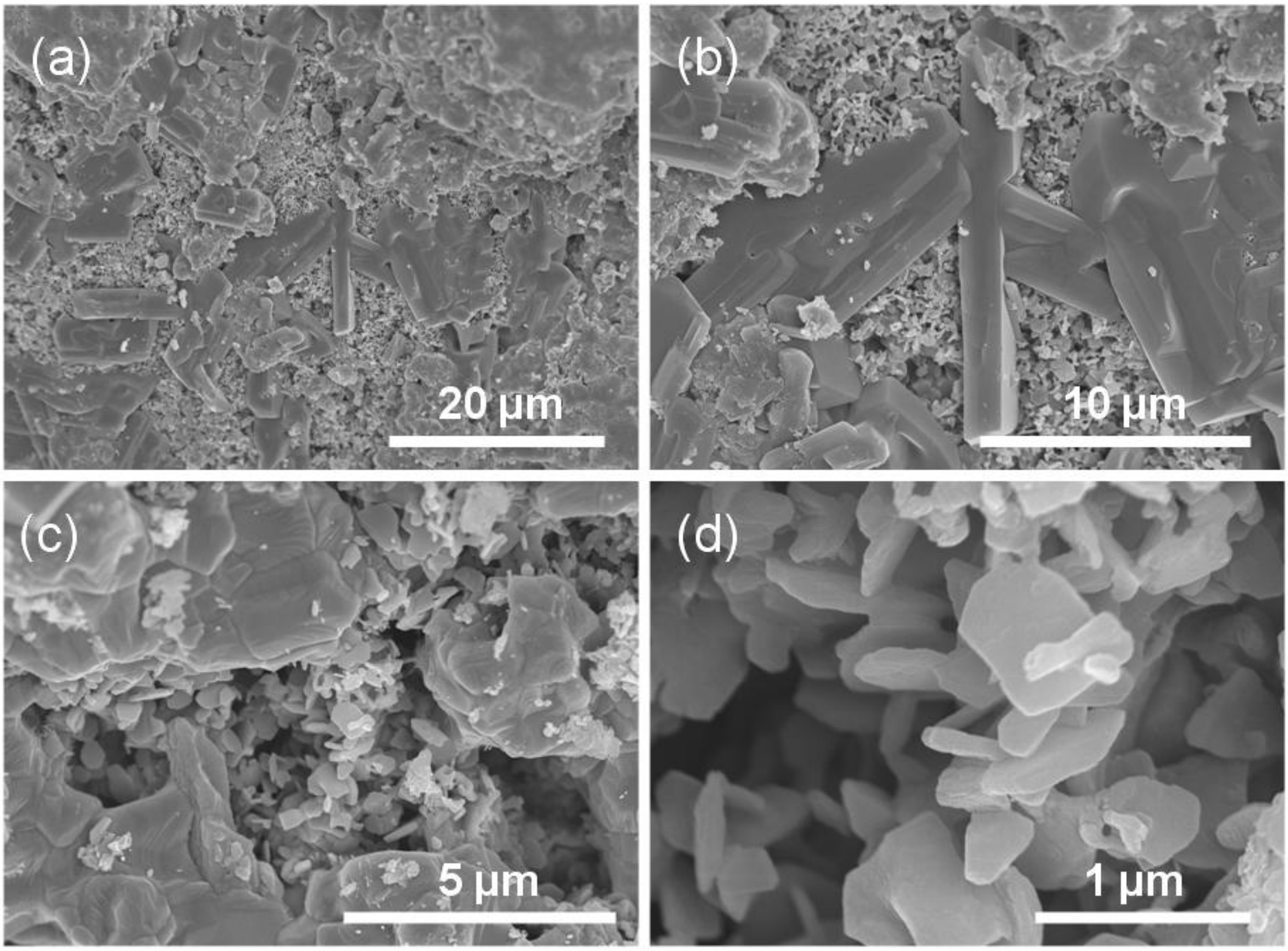

Fig. S27 SEM images of the 82.5 wt% CuO/Al_2O_3 after multiple redox cycles at 900°C. SEM images show that sintering occurred with large grains forming, yet, despite the sintering, the nanoplatelets were preserved in some parts. The 82.5 wt% CuO/Al_2O_3 was calcined from Cu-Al LDH, $Cu^{2+}:Al^{3+}=3:1$, total concentration of 1 M, precipitated with a mixture of NaOH and Na_2CO_3 (0.5 M of each). The content of sodium in the fresh 82.5wt% CuO/Al_2O_3 was 1.4 wt%, as measured by ICP-AES.

5.4 SEM/STEM images of fresh and used 82.5 wt% CuO/Al_2O_3 (Fig. S28)

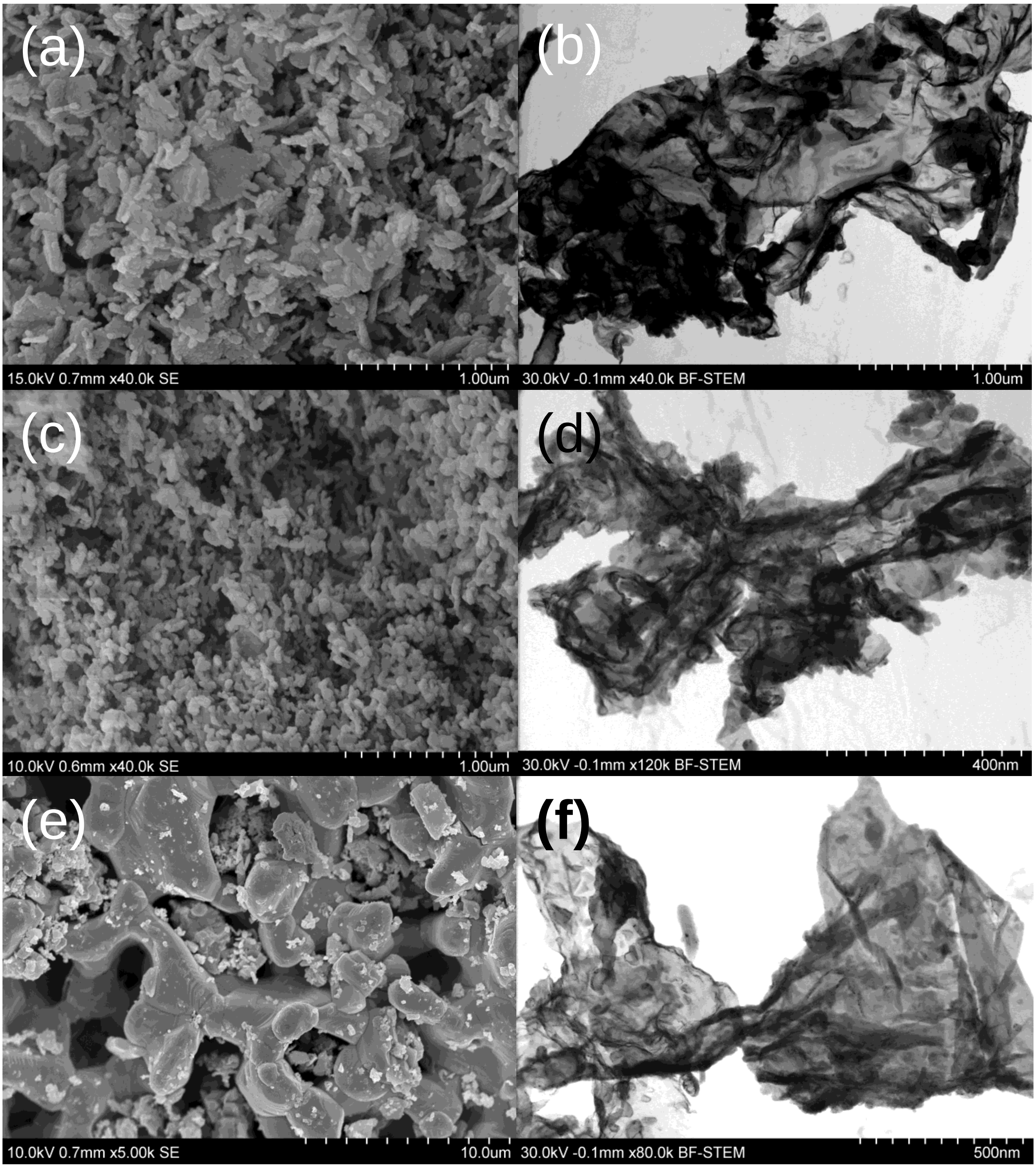

Fig. S28 SEM/STEM images of (a-b) fresh as calcined 82.5 wt% CuO/Al_2O_3, (c-d) used after 20 redox cycles at 800°C, (e-f) used after 20 redox cycles at 950°C. The 82.5 wt% CuO/Al_2O_3 was calcined from Cu-Al LDH, Cu^{2+}:Al^{3+}=3:1, total concentration of 1 M, precipitated with a mixture of NaOH and Na_2CO_3 (0.5 M of each). The content of sodium in the fresh 82.5wt% CuO/Al_2O_3 was 1.4 wt%, as measured by ICP-AES.

5.5 XRD patterns of 82.5 and 60 wt% CuO/Al_2O_3 after multiple redox cycles over 800-1000°C (Fig. S29)

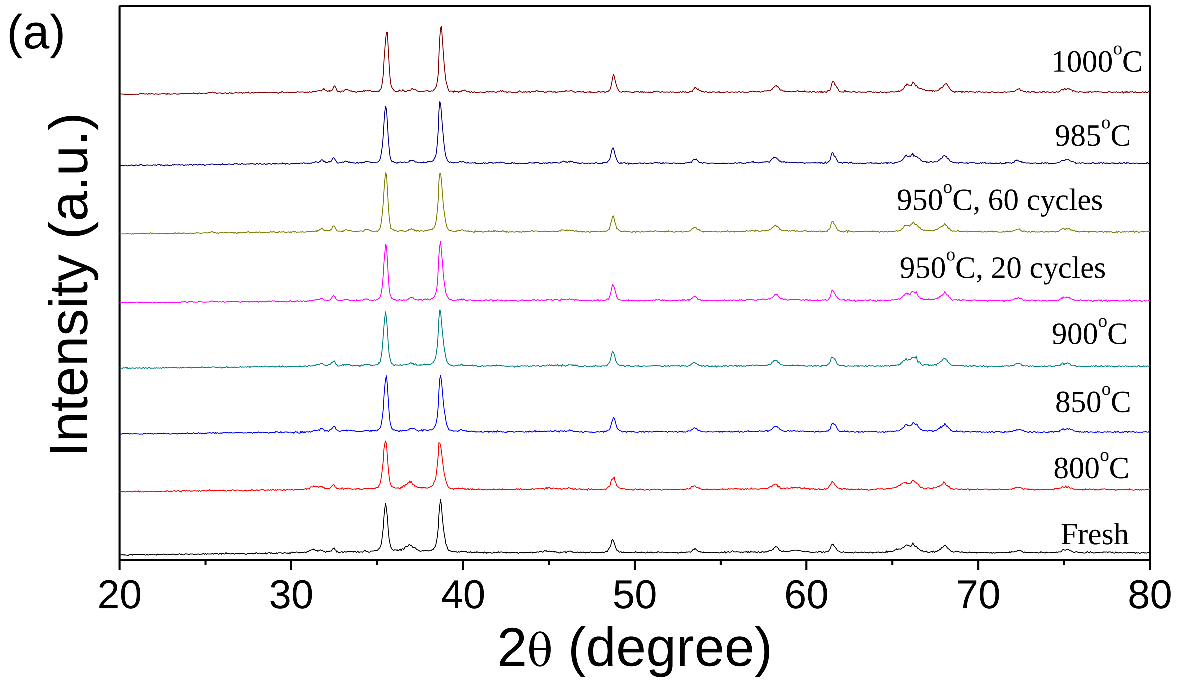

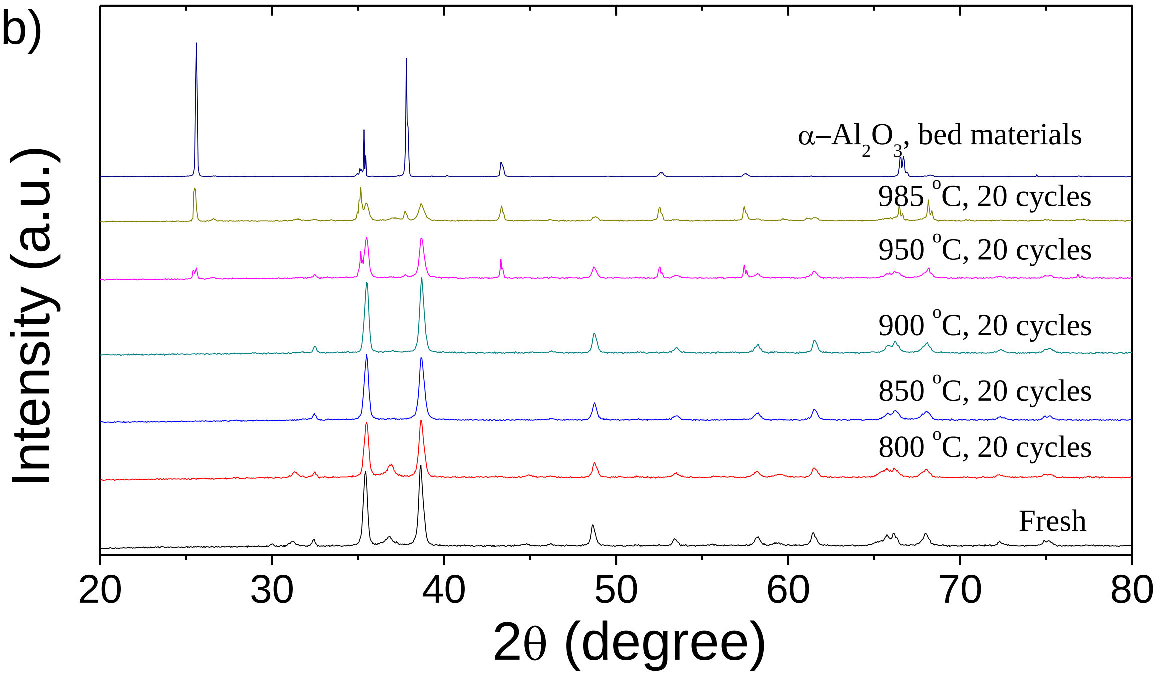

Fig. S29 XRD patterns of used particles exposed to consecutive cycles of reduction and oxidation with CO as gaseous fuel. (a) 60wt% CuO/Al_2O_3, (b) 82.5wt% CuO/Al_2O_3. The temperature and number of cycles are marked above the line, or 20 cycles if not specified. The crystalline phases were maintained over all reaction conditions without further formation of copper aluminate, even for the loading of 82.5 wt% at excessive reaction temperatures when agglomeration occurred. The α–alumina peaks in the patterns for the material cycled at 950 and 985 ºC arise from the bed material which was trapped within the agglomerates formed in the reactor. The 82.5 wt% CuO/Al_2O_3 was calcined from Cu-Al LDH, Cu^{2+}:Al^{3+}=3:1, total concentration of 1 M, precipitated with a mixture of NaOH and Na_2CO_3 (0.5 M of each). The 60 wt% CuO/Al_2O_3 was calcined from Cu-Al LDH, with Cu^{2+}:Al^{3+}=1:1 total concentration of 2 M, precipitated with a mixture of NaOH and Na_2CO_3 (1 M of each). The content of sodium in the fresh 82.5wt% and 60wt% CuO/Al_2O_3 was 1.4 wt% and 7.9 wt%, respectively, as measured by ICP-AES.

5.6 Oxygen storage capacity of 60 wt% CuO/Al_2O_3 after multiple redox cycles (Fig. S30)

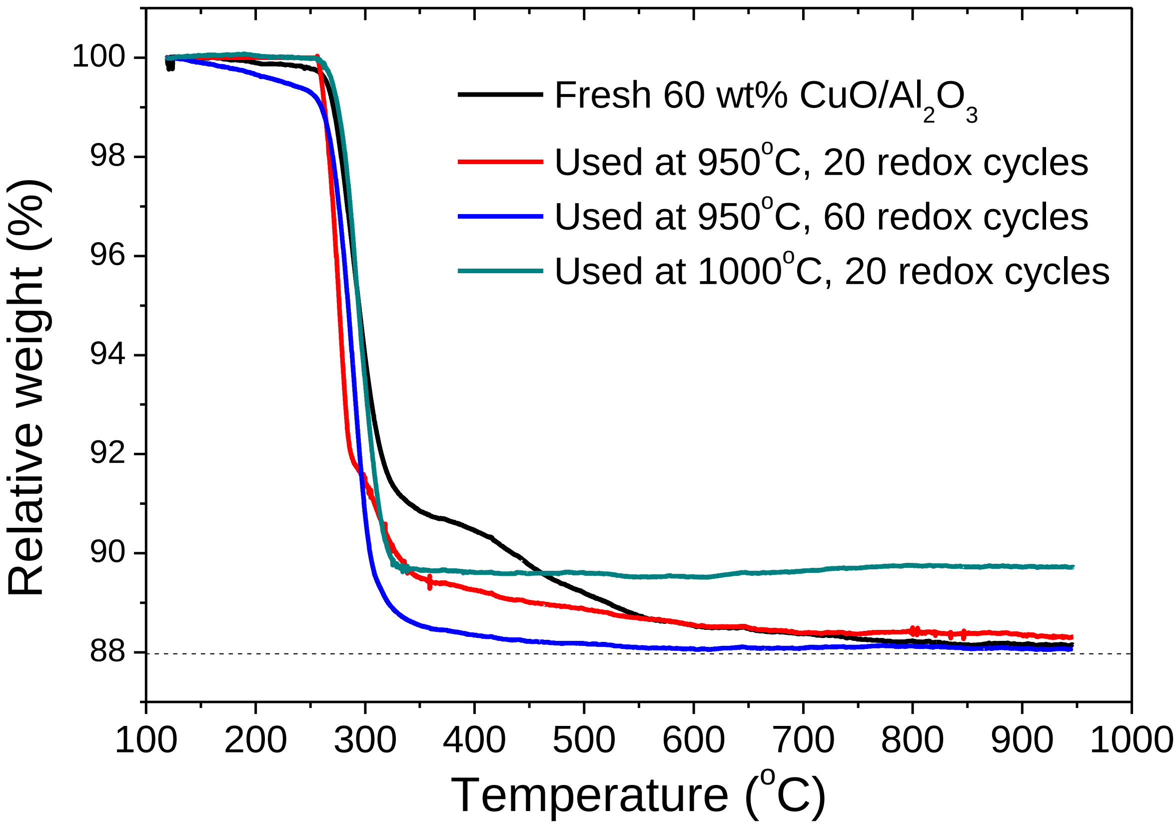

Fig. S30 H_2-TPR of fresh and used particles after multiple redox cycles. The dashed line indicates the weight of completely reduced oxygen carrier for a nominal loading of 60 wt%, and assuming that copper is only present as metallic Cu. Slight loss of oxygen storage capacity occurred at 1000°C indicating slight sintering, still the oxygen storage capacity was as high as ~10wt%. The Cu-based mixed metal oxides with nominal CuO loading of 60 wt% was calcined from Cu-Al LDH, with $Cu^{2+}:Al^{3+}=1:1$ total concentration of 2 M, precipitated with a mixture of NaOH and Na_2CO_3 (1 M of each). The content of sodium in the fresh 60wt% CuO/Al_2O_3 was 7.9 wt%, as measured by ICP-AES.

5.7 SEM images of 60 wt% CuO/Al_2O_3 exposed to 60 redox cycles at 950°C (Fig. S31)

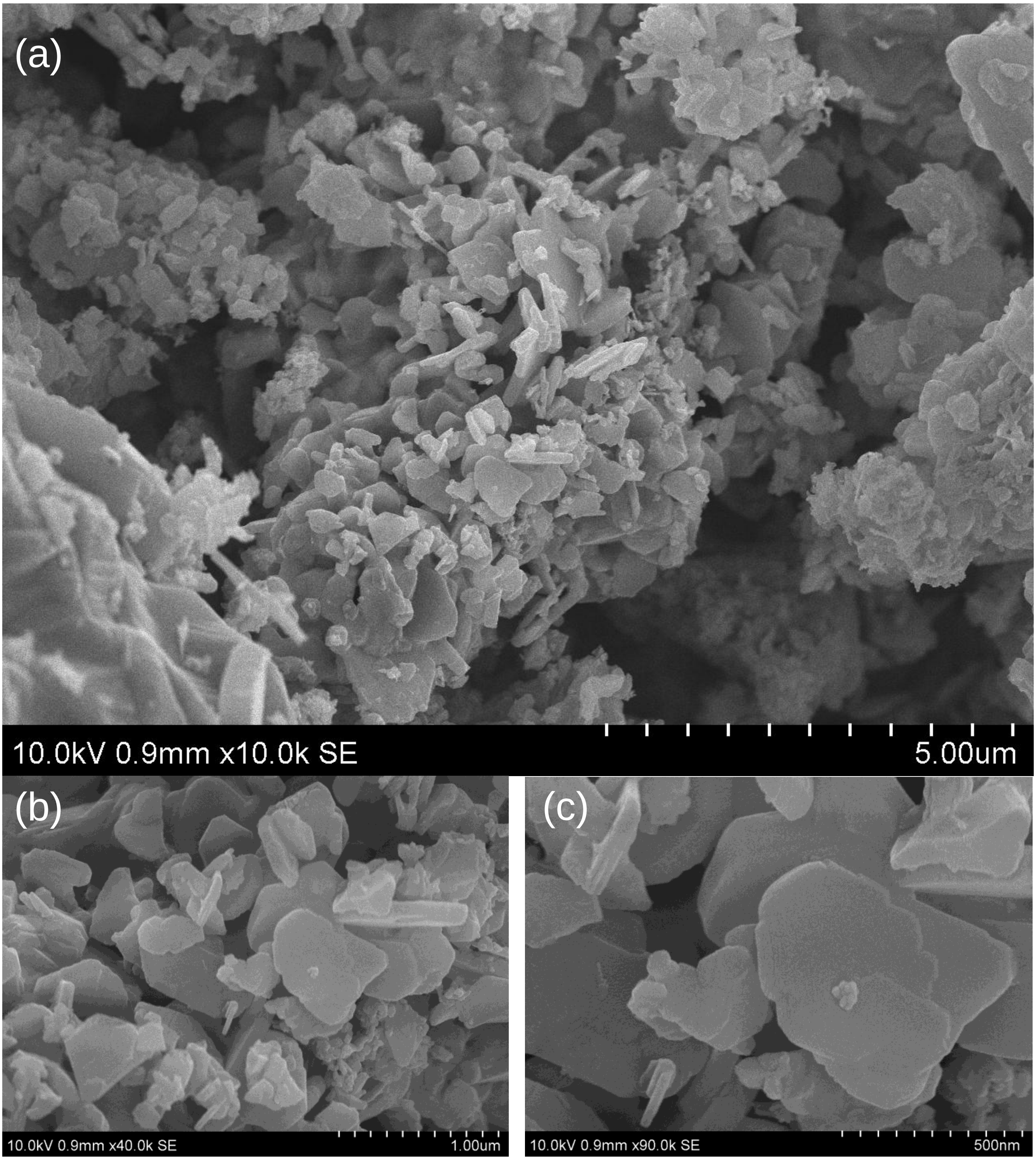

Fig. S31 SEM images of CuO/Al_2O_3 nanocomposite after 60 redox cycles at 950°C in a fluidised bed. Large grains were formed due to sintering in some regions, which are mixed with regions where nanoplatelets could still be observed. The scale bar is marked by the 10 grids at bottom right. The Cu-based mixed metal oxides with nominal CuO loading of 60 wt% was calcined from Cu-Al LDH, with Cu^{2+}:Al^{3+}=1:1 total concentration of 2 M, precipitated with a mixture of NaOH and Na_2CO_3 (1 M of each). The content of sodium in the fresh 60wt% CuO/Al_2O_3 was 7.9 wt%, as measured by ICP-AES.

5.8 STEM image of 60 wt% CuO/Al_2O_3 exposed to multiple redox cycles at 950°C (Fig. S32)

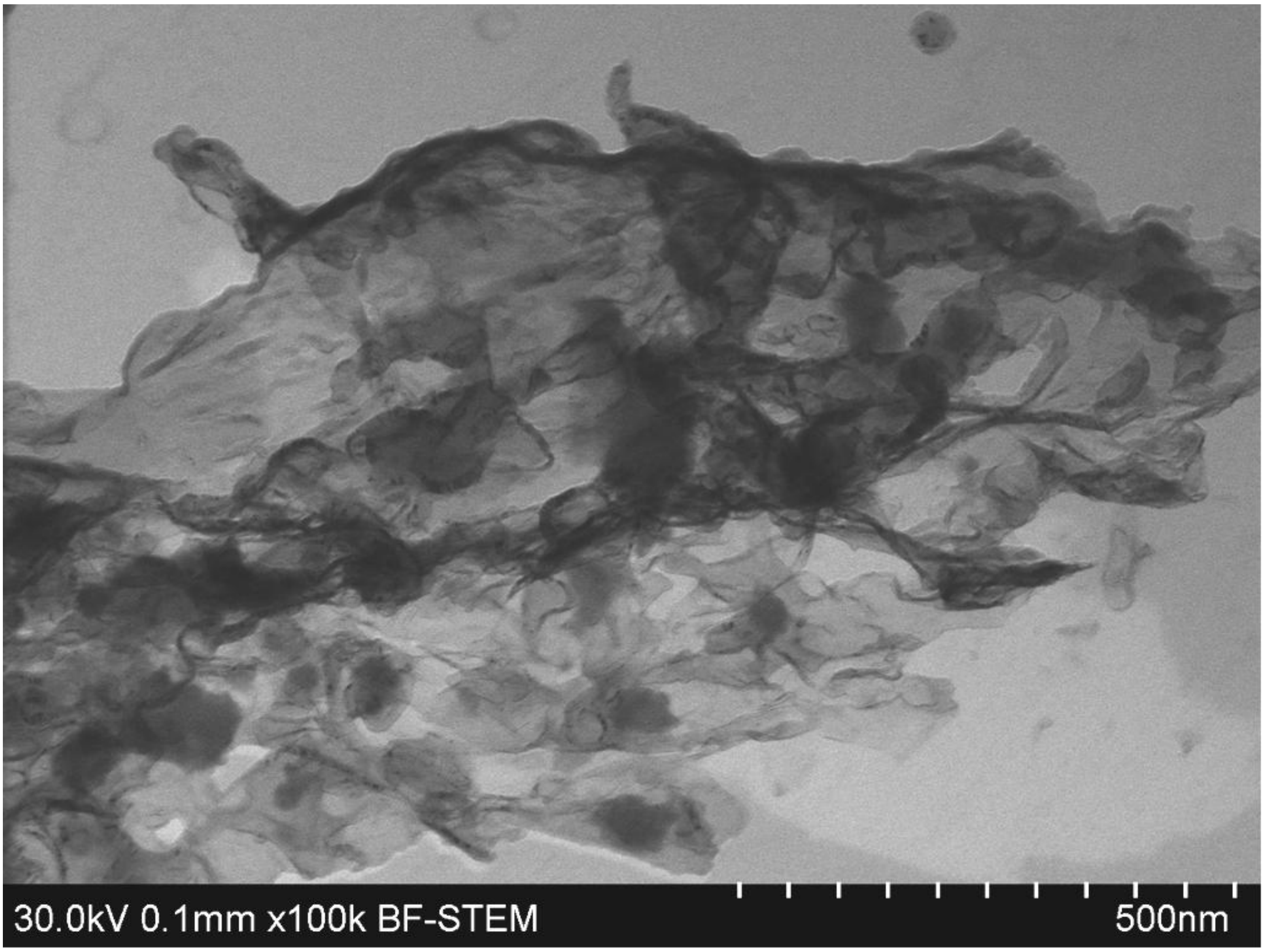

Fig. S32 STEM image of 60 wt% CuO/Al_2O_3 oxygen carrier exposed to 20 redox cycles at 950°C in a fluidised bed. The scale bar is marked by the 10 grids at bottom right. The CuO crystals were still well dispersed in the support matrix (although crystallite size was not uniform, about 30-40 nm, as determined by XRD). The Cu-based mixed metal oxides with nominal CuO loading of 60 wt% was calcined from Cu-Al LDH, with Cu^{2+}:Al^{3+}=1:1 total concentration of 2 M, precipitated with a mixture of NaOH and Na_2CO_3 (1 M of each). The content of sodium in the fresh 60wt% CuO/Al_2O_3 was 7.9 wt%, as measured by ICP-AES.